Taylor & Francis
Taylor & Francis Group

Australian Journal of Earth Sciences

An International Geoscience Journal of the Geological Society of Australia

ISSN: 0812-0099 (Print) 1440-0952 (Online) Journal homepage: https://www.tandfonline.com/loi/taje20

Mid- to lower-crustal architecture of the northern Lachlan and southern Thomson orogens: evidence from O–Hf isotopes

K. Waltenberg, S. Bodorkos, R. Armstrong & B. Fu

To cite this article: K. Waltenberg, S. Bodorkos, R. Armstrong & B. Fu (2018) Mid- to lower-crustal architecture of the northern Lachlan and southern Thomson orogens: evidence from O–Hf isotopes, Australian Journal of Earth Sciences, 65:7-8, 1009-1034, DOI: 10.1080/08120099.2018.1463928

To link to this article: https://doi.org/10.1080/08120099.2018.1463928

Published online: 14 May 2018.

AUSTRALIAN JOURNAL OF EARTH SCIENCES
2018, VOL. 65, NO. 7-8, 1009–1034
https://doi.org/10.1080/08120099.2018.1463928

Mid- to lower-crustal architecture of the northern Lachlan and southern Thomson orogens: evidence from O–Hf isotopes

K. Waltenberg[a], S. Bodorkos[a], R. Armstrong[b] and B. Fu[b]

[a]Resources Division, Geoscience Australia, Canberra, ACT, Australia; [b]Research School of Earth Sciences, The Australian National University, Canberra, ACT, Australia

ABSTRACT

The nature of the substrate below the northern Lachlan Orogen and the southern Thomson Orogen is poorly understood. We investigate the nature of the mid- to lower-crust using O and Lu–Hf isotope analyses of zircons from magmatic rocks that intrude these regions, and focus on the 440–410 Ma time window to minimise temporal effects while focussing on spatial differences. Over the entire region, weighted mean $\delta^{18}O$ values range from 5.5 to 9.8‰ (relative to VSMOW, Vienna Standard Mean Oceanic Water), and weighted mean εHf_t range from −8.8 to +8.5. In the northern Lachlan Orogen and much of the southern Thomson Orogen, magmatic rocks with unradiogenic εHf_t (∼−7 to −4) and elevated $\delta^{18}O$ values (∼9 to 10‰) reflect a supracrustal source component that may be common to both orogens. Magmatic rocks intruding the Warratta Group in the western part of the Thomson Orogen also have unradiogenic εHf_t (∼−9 to −6) but more subdued $\delta^{18}O$ values (∼7‰), indicating a distinct supracrustal source component in this region. Some regions record radiogenic εHf and mantle-like $\delta^{18}O$ values, indicative of either a contribution from arc-derived rocks or a direct mantle input. In the northeast Lachlan Orogen Hermidale Terrane, magmatic rocks record mixing of the supracrustal source component with input from a infracrustal or mantle source component (εHf_t as high as +8.5, $\delta^{18}O$ values as low as 5.5‰), possibly of Macquarie Arc affinity. Samples in the west-southwestern Thomson Orogen also record some evidence of radiogenic input (εHf_t as high as −0.5, $\delta^{18}O$ values as low as 6.4‰), possibly from the Mount Wright Arc of the Koonenberry Belt. Overall, our results demonstrate a strong spatial control on isotopic compositions. We find no isotopic differences between the bulk of the Lachlan Orogen and the bulk of the Thomson Orogen, and some indication of similarities between the two.

ARTICLE HISTORY
Received 23 August 2017
Accepted 3 April 2018

KEYWORDS
Thomson Orogen; Lachlan Orogen; Lu–Hf isotopes; oxygen isotopes; zircon; New South Wales; Macquarie Arc; Mount Wright Arc; Warratta Group; Olepoloko Fault

Introduction

The Tasmanides constitute the eastern third of the Australian continent, and broadly record early Paleozoic (*ca* 500 Ma) to early Mesozoic (*ca* 250 Ma) crustal addition to the eastern margin of Precambrian Australia, via arc-related accretion and associated sedimentation (e.g. Cawood & Buchan, 2007; Champion, 2016; Collins, 2002; Glen, 2005; Gray & Foster, 2004).

There exist numerous, but variable, models to explain the current geological configuration of the Tasmanides. Common elements include successive orogenic cycles on an east-facing continental margin (e.g. Burton, 2010; Fergusson & Henderson, 2013; Glen *et al*., 2013; Gray & Foster, 2004; Kirkegaard, 1974; Moresi, Betts, Miller, & Cayley, 2014; Murray & Kirkegaard, 1978; Scheibner, 1973). Current understanding of the Tasmanides is based largely on relatively well-exposed geological relationships in the southern and eastern Tasmanides: the Delamerian Orogen in South Australia, the Lachlan Orogen in Victoria and New South Wales (NSW) and the New England Orogen in northern NSW and southern Queensland (Figure 1).

A major blind spot in understanding the Tasmanides is the Thomson Orogen: a very large region of Queensland and northern NSW. Its location largely coincides with the region now covered by the Mesozoic Eromanga Basin. As such, exposure is scarce, and basement intersections in drill core are sparse. Limited information indicates that Paleozoic metasedimentary and igneous rocks comprise the bulk of geology beneath the Eromanga Basin (Brown, Carr, & Purdy, 2012; Murray, 1994).

Earliest proponents of the term 'Thomson Orogen' used it to distinguish the region from the Lachlan Orogen to the south because so little was known about the geology below the Mesozoic cover (Kirkegaard, 1974; Murray & Kirkegaard, 1978). Evidence for Paleozoic basement, and the position of the Thomson Orogen to the north of, and along strike from, the north–south-striking Lachlan Orogen, suggests that the Thomson Orogen is a northerly extension of the Lachlan

CONTACT K. Waltenberg kathryn.waltenberg@ga.gov.au
Editorial handling: David Purdy

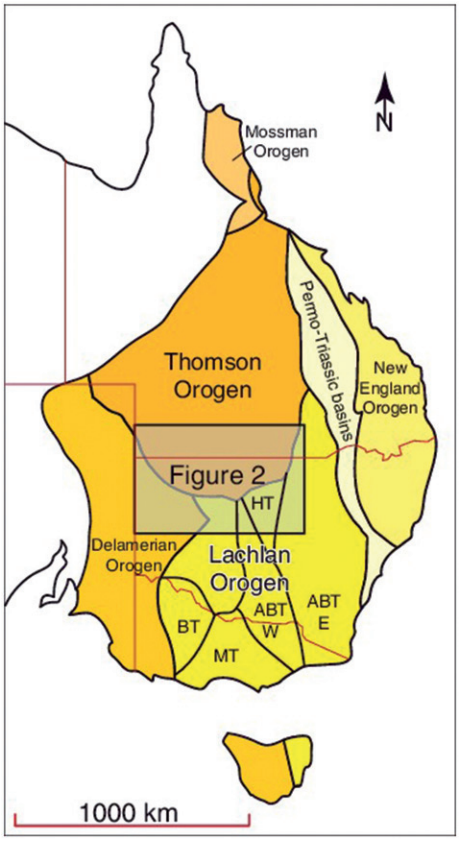

Figure 1. Overview sketch-map showing the location of the study area relative to eastern Australia and the Tasmanides, after Burton (2010), including generalised locations of tectonostratigraphic subdivisions of the Lachlan Orogen after Glen *et al.* (2009). BT, Bendigo Terrane; MT, Melbourne Terrane; ABT, Albury-Bega Terrane (west and east); HT, Hermidale Terrane.

Orogen. This remains to be fully tested. Indeed, there are multiple interpretations of the relationship between the Lachlan Orogen and the Thomson Orogen (e.g. Burton, 2010; Glen, 2013; Moresi *et al.*, 2014). Just as the Lachlan Orogen is subdivided into multiple subdomains (e.g. Glen *et al.*, 2013; Glen, Percival, & Quinn, 2009; Seymour & Calver, 1995; VandenBerg *et al.*, 2000), the size of the Thomson Orogen suggests that it is likely to consist of multiple subdomains with contrasting origins.

The widespread usage of the provincial entities Lachlan Orogen and Thomson Orogen in NSW implies the existence of a boundary between the two. Kirkegaard (1974) proposed the boundary between the Thomson Orogen and the Lachlan Orogen to be the 'Darling Lineament' because it marked a change in structural trend. Wellman (1976) first described a boundary between two distinct gravity domains, which occupy the current locations of the Thomson and Lachlan orogens (Murray & Kirkegaard, 1978). The location of this proposed boundary, now named the Olepoloko Fault and extensions, has largely been upheld in more recent investigations (e.g. Glen *et al.*, 2013), although its status as the boundary between the Thomson Orogen and Lachlan Orogen remains debated (e.g. Burton, 2010; Glen *et al.*, 2013; Moresi *et al.*, 2014).

The north-dipping Olepoloko Fault occurs along the southwestern margin of the southern Thomson Orogen, from north of the Koonenberry Belt, trending south-southeast to the Cuttaburra region (Figure 2; Glen *et al.*, 2013; Greenfield, Gilmore, & Mills, 2010). It separates the Warratta Group of the Thomson Orogen from the Teltawongee Group in the Koonenberry Belt of the Delamerian Orogen (Greenfield *et al.*, 2010).

Farther to the east, geological and geophysical evidence for continuation of the Olepoloko Fault becomes scarce, in part due to cover by the Siluro-Devonian Cobar Supergroup (Glen *et al.*, 2009). Glen *et al.* (2009) inferred that the Olepoloko Fault continues to the east, south around the Louth Volcanics, then along the northern faults of the Louth-Eumarra shear zone, namely the Little Mountain Fault and Mount Oxley Fault (Figure 2). Other authors dispute the Olepoloko Fault as the boundary between the Lachlan Orogen and the Thomson Orogen, and even the existence of the Thomson Orogen as a separate provincial entity (e.g. Burton, 2010). For clarity, we refer to the Olepoloko Fault and its inferred extensions, which run along the boundary between the two orogens as shown in Figure 1, as the Lachlan–Thomson Boundary Structures (LTBS).

The contiguity or otherwise of the northern Lachlan Orogen–southern Thomson Orogen has implications for mineral systems and prospectivity. The exposed northern Lachlan Orogen is exceptionally well endowed with mineral deposits. Contiguity of crust across the Olepoloko Fault raises the possibility that similar mineral systems might exist under cover in the Thomson Orogen. Alternatively, if the Thomson Orogen represents fundamentally different crust, this has different implications for mineral prospectivity.

Here, we use the oxygen and lutetium–hafnium isotopic systems in zircon to interrogate the nature of the mid- to lower-crustal substrate in the northern Lachlan and southern Thomson orogens, in particular, whether there is a fundamental difference between substrate to the Lachlan and Thomson orogens, and to determine whether the LTBS defines the boundary between two isotopically distinct crustal substrates. We confine our investigation to a narrow time window (440–410 Ma) to limit the effects of crustal evolution on the isotopic results.

Geological setting

The Lachlan and Thomson orogens are broad (>600 km east–west, Figure 1), and outcrop is poor. Over most of both orogens, the oldest rocks exposed are Ordovician turbiditic rocks (although Cambrian greenstone belts outcrop in Victoria; Crawford & Keays, 1978), and the nature of their substrate is poorly understood. The eastern margin of both orogens is obscured by the predominantly Permian Bowen, Gunnedah and Sydney basins.

Glen *et al.* (2009) divided the Lachlan Orogen into several tectonostratigraphic terranes (Figure 1). The Albury-Bega Terrane is the largest of these by area, spanning the entire north–south extent of the Lachlan Orogen, and is ~500 km

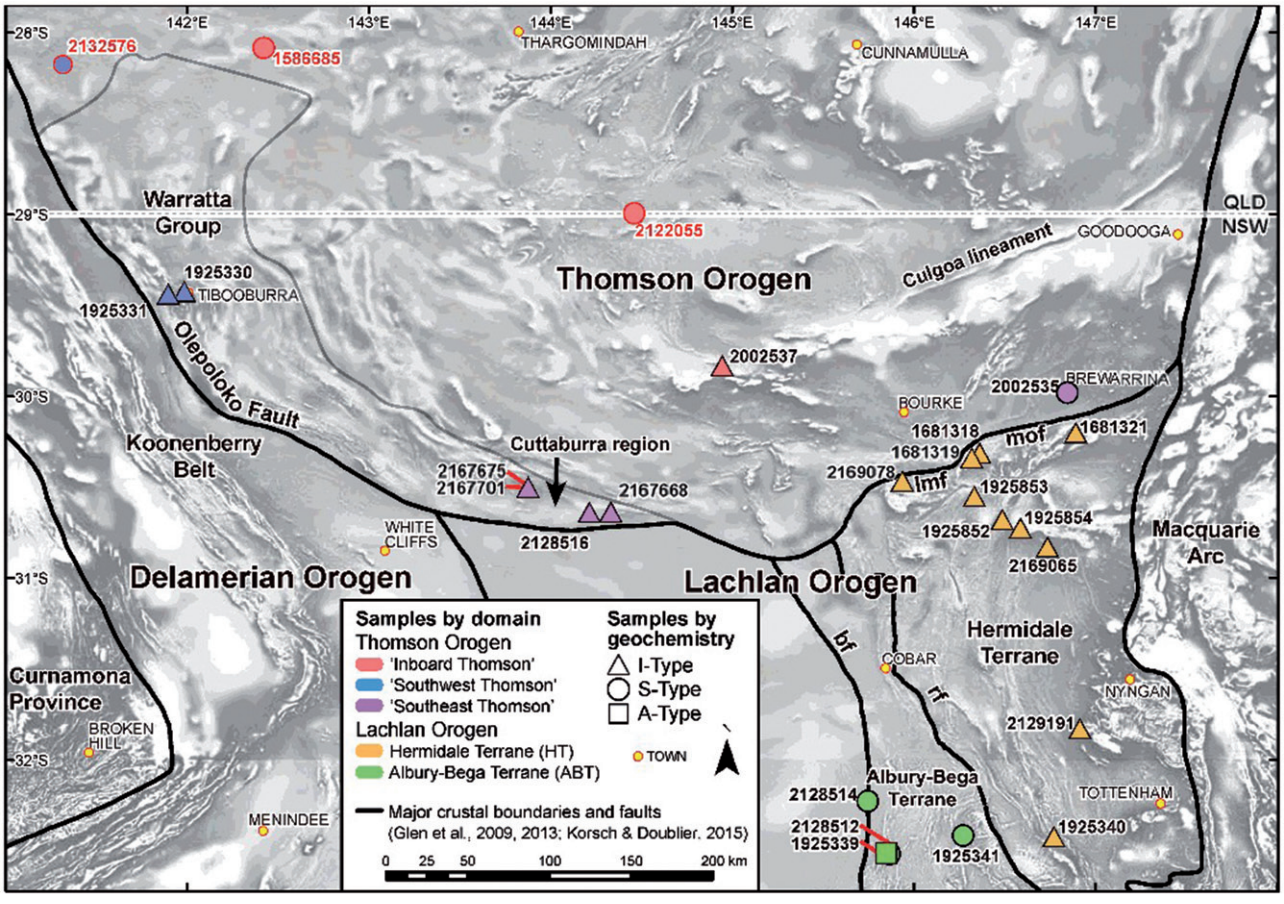

Figure 2. Map of the southern Thomson Orogen and surrounds, showing sample locations. Samples are coloured by domain: red, 'Inboard Thomson'; blue, 'Southwest Thomson'; purple, 'Southeast Thomson'; orange, Hermidale Terrane; green, Albury-Bega Terrane. Symbols reflect the geochemistry of the samples: triangle, I-Type; circle, S-type; square, A-type. Samples outlined in red and with red sample numbers are from other publications—refer to text. Major crustal boundaries and faults are marked with black lines, following those illustrated in Glen *et al.* (2009, 2013) and Korsch and Doublier (2015). The Lachlan–Thomson Boundary Structures (LTBS) consist of the Olepoloko Fault, lmf, Little Mountain Fault and mof, Mount Oxley Fault. bf, Boothergandra Fault; rf, Rookery Fault System. Towns are marked by small yellow spots, and the QLD–NSW border is marked by a dashed line.

east–west in places; this terrane has been divided into west and east components. The Macquarie Arc, an extensive volcanic arc system (although alternate models exist, e.g. Quinn, Percival, Glen, & Xiao, 2014), active during the Ordovician and earliest Silurian (*ca* 489–437 Ma, Percival & Glen, 2007), occurs in belts from the eastern margin of the western Albury-Bega Terrane across the northern part of much of the eastern Albury-Bega Terrane (Figure 2). These belts are thought to represent a single magmatic arc that has subsequently been disjointed by accretion and rifting in the Silurian and Devonian (Percival & Glen, 2007). In the north, abutting the southeastern Thomson Orogen, the Hermidale Terrane is distinguished from the Albury-Bega Terrane by the absence of Upper Ordovician units and the presence of mafic volcanic rocks (Glen *et al.*, 2009).

Subdivision of the Thomson Orogen has proven to be more difficult owing to thick Mesozoic–Cenozoic cover. Most outcropping rock in the Thomson Orogen occurs in the far north, in the Greenvale, Charters Towers and Anakie provinces. Sparse exposure of igneous and metasedimentary rocks outcrop around the Eulo Ridge region in southern Queensland (Bultitude & Cross, 2013), the Tibooburra region in northwest NSW (Greenfield *et al.*, 2010), and in the Louth region near the boundary with the Lachlan Orogen (Glen *et al.*, 2013). Elsewhere, direct information about pre-Mesozoic geology comes from drill core (Brown *et al.*, 2012; Murray, 1994). Carr, Purdy, and Brown (2014) and Purdy, Cross, Brown, Carr, and Armstrong (2016) made use of the geological information available from drill core to map the distribution of units, and U–Pb zircon dating to determine their provenance.

Magmatic rocks are found close to the surface in the southern Thomson Orogen near the Culgoa lineament: an elongate, narrow aeromagnetic anomaly that represents a significant, deep zone of faulting that is associated with a basement high (Figure 2; Doublier, Purdy, Hegarty, Nicoll & Zwingmann, 2018; Hegarty & Doublier, 2015). Drilling intersected intrusive rock at 184 m (Burtt & Lockheed, 2008).

The upper Cambrian to Lower Ordovician metasedimentary Warratta Group (Figure 2) has very restricted outcrop in the southwest Thomson Orogen, but it does have a distinct, relatively high magnetic character, which distinguishes it

from surrounding units (Greenfield *et al*., 2010). This distinction suggests that the Warratta Group has a much more extensive sub-surface extent, as interpreted by Purdy, Hegarty, and Doublier (2018). Magmatic rocks of the Tibooburra Suite and Evelyn Creek volcanics intrude the outcropping Warratta Group (Greenfield *et al*., 2010).

The southwestern Thomson Orogen abuts the upper Precambrian to middle Cambrian sedimentary–volcanic Koonenberry Belt, an exposed region of the Delamerian Orogen (Greenfield *et al*., 2010). The Koonenberry Belt records development of calc-alkaline volcanism of the Mount Wright Volcanics, which are interpreted to represent a volcanic arc (Greenfield, Musgrave, Bruce, Gilmore, & Mills, 2011). The lower–middle Cambrian Mount Wright Volcanics are only exposed in the Mount Wright region of the Koonenberry Belt (Greenfield *et al*., 2010). Greenfield *et al*. (2011) estimated the overall volume, based on aeromagnetic and gravity data and supported by drilling in the Bancannia Trough, to be much more extensive. Gatehouse (1986) suggested that the lower Cambrian Mooracoochie Volcanics in the Warburton Basin to the north may be a northward extension of the Mount Wright Arc.

Scientific approach

The mid–lower crust is not directly observable, although it can be imaged in seismic-reflection studies. The approach taken here is to use felsic magmatic rocks as 'deep crustal probes.' These rocks are interpreted to form by melting within the mid to lower crust before crystallising in the upper crust.

Granite formation is a chemically and isotopically complex process. Mantle-derived mafic magmas can be involved both as a primary isotopic source in an assimilation and fractionation crystallisation sequence, or can behave primarily as a thermal source, driving partial melting of mid–lower-crustal rocks of potentially diverse isotopic composition (Chappell & Stephens, 1988; Gray, 1984; Kemp, Wormald, Whitehouse, & Price, 2005b).

Nevertheless, commonly the only component of these processes that we can physically interact with is the granite itself. Granites should have isotopic signatures that reflect the processes and components that contributed to their formation, and measuring the isotopic composition of accessory minerals in these rocks is one of few insights into their source regions (Keay, Collins, & McCulloch, 1997; Kemp, Whitehouse, Hawkesworth, & Alarcon, 2005a; Kemp *et al*., 2005b, Kemp *et al*., 2008). However, final isotopic compositions preserved in these minerals do not necessarily uniquely prescribe the processes and inputs into granite generation (Chappell, 1979). Notwithstanding the possible complexity of petrogenetic processes, isotopic characterisation is particularly valuable in our study area because exposure is so poor that there is no realistic opportunity to collect suites (*sensu stricto* Chappell & White, 1992) of chemically and isotopically related rocks.

Pioneering studies (e.g. Bennett & DePaolo, 1987) and more recent applications (e.g. Champion, 2013; Gardiner *et al*., 2017; Mole *et al*., 2013; Mole *et al*., 2014) show the potential to use the isotopic character of granites to 'map' the deep crust. Here, we use the O and Hf isotopic signature preserved in zircons from magmatic rocks to investigate character and possible variability of the deep crust beneath the northern Lachlan–southern Thomson Orogens. This study complements other isotopic studies focussed on the Thomson Orogen (Cross *et al*., 2018; Purdy *et al*., 2016).

As indicated above, various tectonic models exist for the Tasmanides, and for the relationship between the Lachlan Orogen and the Thomson Orogen. Some of these models have different implications for the nature of the deep crust. Results from this study may, therefore, provide some testing of these models.

Analytical methods

The results of SHRIMP U–Pb, SHRIMP oxygen isotope and MC-LA-ICP-MS Lu–Hf isotope analyses of zircons from 22 samples are presented here. All U–Pb isotope analyses were performed by other researchers, as cited on a sample-by-sample basis (see Table 1). U–Pb isotope analyses of all zircons used in this study were collected as part of the Geoscience Australia (GA) geochronology program, and the relevant epoxy zircon mounts and grain images were available from the GA mount archive.

Oxygen, then Lu–Hf isotope analyses were performed sequentially on spots from the U–Pb magmatic age population. These isotopic analyses were performed through the SHRIMP and LA-ICP-MS facilities at the Research School of Earth Sciences (RSES) at The Australian National University. The number of O and Lu–Hf isotopic data points retrieved from each sample was directly limited by the number of precursor U–Pb isotope analyses made on zircon from that sample, and by the quality of those zircons. Not all U–Pb isotope analytical spots are suitable for follow-up O and Lu–Hf isotope analyses owing to the larger sampling volume required (see below). This requirement, together with the fact that, in many cases, follow-up O and Lu–Hf isotope analyses were not envisaged by the analysts at the time of original U–Pb isotope analyses, means that for some samples the number of suitable targets for O and Lu–Hf isotope analyses was limited. Figure 3 illustrates the geometric difference between U–Pb, O and Lu–Hf isotope analytical spots. Analytical O and Lu–Hf session data and full isotopic data tables are provided in the Supplementary Papers (Appendix A).

Oxygen isotope analyses were performed on either of the SHRIMP II or SHRIMP SI instruments at RSES. Ickert *et al*. (2008) describe the general procedures for SHRIMP oxygen isotope analyses at the RSES facilities. Co-mounted TEMORA2 zircons are used as the primary reference material in all sessions, and other reference zircons were analysed if they were present on the sample mounts. The ablation pit size was on average 25 μm, which excavated pits less than 1 μm deep over the course of the analysis. $\delta^{18}O$ values are reported relative to VSMOW (Vienna Standard Mean Oceanic Water; Baertschi, 1976).

Table 1. Sample information and summary isotopic results.

GA sample no.	GDA94 latitude	GDA94 longitude	Age (Ma) ± 95% CI	Stratigraphic name/ informal identifier	Lithology	$\delta^{18}O$ (‰ VSMOW) Weighted mean ± 95% CI	MSWD	$\delta^{18}O$ (‰ VSMOW) Arithmetic mean ± 2SD	εHf_t Weighted mean ± 95% CI	MSWD	εHf_t Arithmetic mean ± 2SD
Albury-Bega Terrane											
1925341	−32.4210	146.2720	427.2 ± 2.4[a]	Erimeran Granite	Felsic porphyritic granite	9.39 ± 0.56	12	9.37 ± 1.71	−6.9 ± 0.6	1.6	−6.8 ± 2.1
1925339	−32.5172	145.8457	420.0 ± 2.4[a]	Boolahbone Granite	Granodiorite	9.72 ± 0.26	4.8	9.71 ± 0.69	−7.2 ± 1.2	3.4	−7.2 ± 3.2
2128514	−32.2298	145.7455	425.7 ± 2.4[b]	Thule Granite	Felsic muscovite granite	9.44 ± 0.13	3.2	9.44 ± 0.54	−5.7 ± 0.7	0.66	−5.6 ± 3.0
2128512	−32.5207	145.8654	422.8 ± 2.6[b]	Mount Halfway Volcanics	Porphyritic quartz–feldspar rhyolite	9.78 ± 0.23	11	9.78 ± 1.03	−5.9 ± 1.4	1.6	−5.1 ± 5.1
Hermidale Terrane											
1925340	−32.4285	146.7678	420.6 ± 2.8[a]	Yellow Mountain Granite	Granite	7.08 ± 0.69	9.4	7.12 ± 1.60	−3.4 ± 1.4	1.3	−2.2 ± 5.6
1925854	−30.7268	146.584	422.6 ± 2.4[a]	Glenariff Granite	Coarse-grained syenogranite	6.33 ± 0.32	4.7	6.33 ± 1.04	−0.2 ± 1.5	7.2	−0.5 ± 4.7
2169065	−30.8347	146.7325	421.9 ± 2.9[c]	Granite, Glen Idyll Prospect	Biotite granite	5.66 ± 0.22	3.2	5.66 ± 0.82	+5.1 ± 0.6	1.1	+5.4 ± 2.7
1925852	−30.6837	146.4829	416.8 ± 2.5[a]	Byrock Granite	Porphyritic coarse-grained granite	8.01 ± 0.48	7.4	8.00 ± 1.28	+1.4 ± 1.4	0.69	+2.2 ± 3.8
1925853	−30.5570	146.3310	430.4 ± 2.6[a]	Knightvale Granite	Medium-grained granodiorite	6.70 ± 0.45	4.9	6.71 ± 1.05	+1.8 ± 1.8	2.4	+1.2 ± 3.4
2169078	−30.4720	145.9352	417.8 ± 3.2[c]	Galambo Granite	Granite	6.39 ± 0.17	2.8	6.39 ± 0.77	+1.9 ± 0.5	0.95	+2.3 ± 3.1
1681318	−30.3187	146.3589	235.2 ± 1.5[d]	Midway Granite	Felsic granodiorite	6.24 ± 0.18	7.9	6.25 ± 0.81	+4.0 ± 0.6	1.5	+4.2 ± 3.4
1681319	−30.3448	146.3166	230.8 ± 1.4[d]	Quartz porphyry dyke, Doradilla	Quartzo-feldspathic porphyry	6.33 ± 0.20	11	6.34 ± 0.92	+2.1 ± 0.5	1.4	+1.9 ± 2.7
1681321	−30.2049	146.8881	408.9 ± 2.4[d]	Mount Kelly Granite	Granite	5.52 ± 0.16	6.5	5.52 ± 0.72	+8.5 ± 0.5	0.9	+8.6 ± 2.2
2129191	−31.8330	146.9107	442.1 ± 2.1[e]	Honeybugle Complex	Hornblende–quartz–pyroxene diorite	6.02 ± 0.17	1.6	6.02 ± 0.58	+8.0 ± 0.5	1.4	+7.9 ± 2.6
Southwest Thomson Orogen											
1925330	−29.4305	141.9833	420.5 ± 3.2[a]	Tibooburra Granodiorite	Medium-grained granodiorite	6.51 ± 0.21	12	6.51 ± 1.51	−1.8 ± 0.5	2.7	−1.9 ± 4.1
1925331	−29.4432	141.8962	420.2 ± 3.3[a]	Dynamite Tank Granodiorite	Hornblende diorite	6.42 ± 0.22	4.9	6.42 ± 1.00	−0.5 ± 0.2	1.2	−0.5 ± 2.3
Southeast Thomson Orogen											
2167675	−30.5062	143.8747	428.2 ± 3.1[g]	F1 granite, Cuttaburra	Medium-grained biotite granite	6.94 ± 0.23	6.0	6.94 ± 1.13	−6.7 ± 0.7	2.2	−6.8 ± 3.7
2167701	−30.5062	143.8758	424.5 ± 4.9[g]	F1 granitic dyke, Cuttaburra	Leucocratic fine to medium-grained granite	6.86 ± 0.44	7.9	6.87 ± 1.23	−6.9 ± 1.4	3.0	−6.9 ± 3.9
2128516	−30.6448	144.2132	428.3 ± 2.8[b]	Granite, Cuttaburra	Felsic biotite granite	7.33 ± 0.16	3.9	7.33 ± 0.62	−6.8 ± 1.6	1.8	−6.8 ± 4.0
2167668	−30.6425	144.3309	429.0 ± 8.5[g]	Diorite, Cuttaburra	Medium–grained biotite–quartz diorite	6.93 ± 0.69	8.3	6.94 ± 1.30	−8.8 ± 2.1	2.8	−8.6 ± 3.6
2002535	−29.9836	146.8437	420.9 ± 2.3[f]	Brewarrina Granite	Medium–grained biotite–cordierite granite	9.16 ± 0.23	5.3	9.16 ± 1.03	−6.5 ± 0.5	2.8	−6.5 ± 2.7
Inboard Thomson Orogen											
2002537	−29.8390	144.9439	401.8 ± 3.1[f]	Tinchelooka Diorite	Porphyritic monzodiorite	6.25 ± 0.27	4.1	6.25 ± 0.92	+4.9 ± 0.5 −1.9 ± 1.8	1.2 0.03	+4.9 ± 1.7 −1.9 ± 0.2

Ages from: [a] Black (2007), [b] Chisholm *et al.* (2014), [c] Fraser, Kositcin & Thorne (in prep), [d] Black (2006), [e] Fraser *et al.* (2014), [f] Bodorkos *et al.* (2013), [g] Armistead and Fraser (2015).

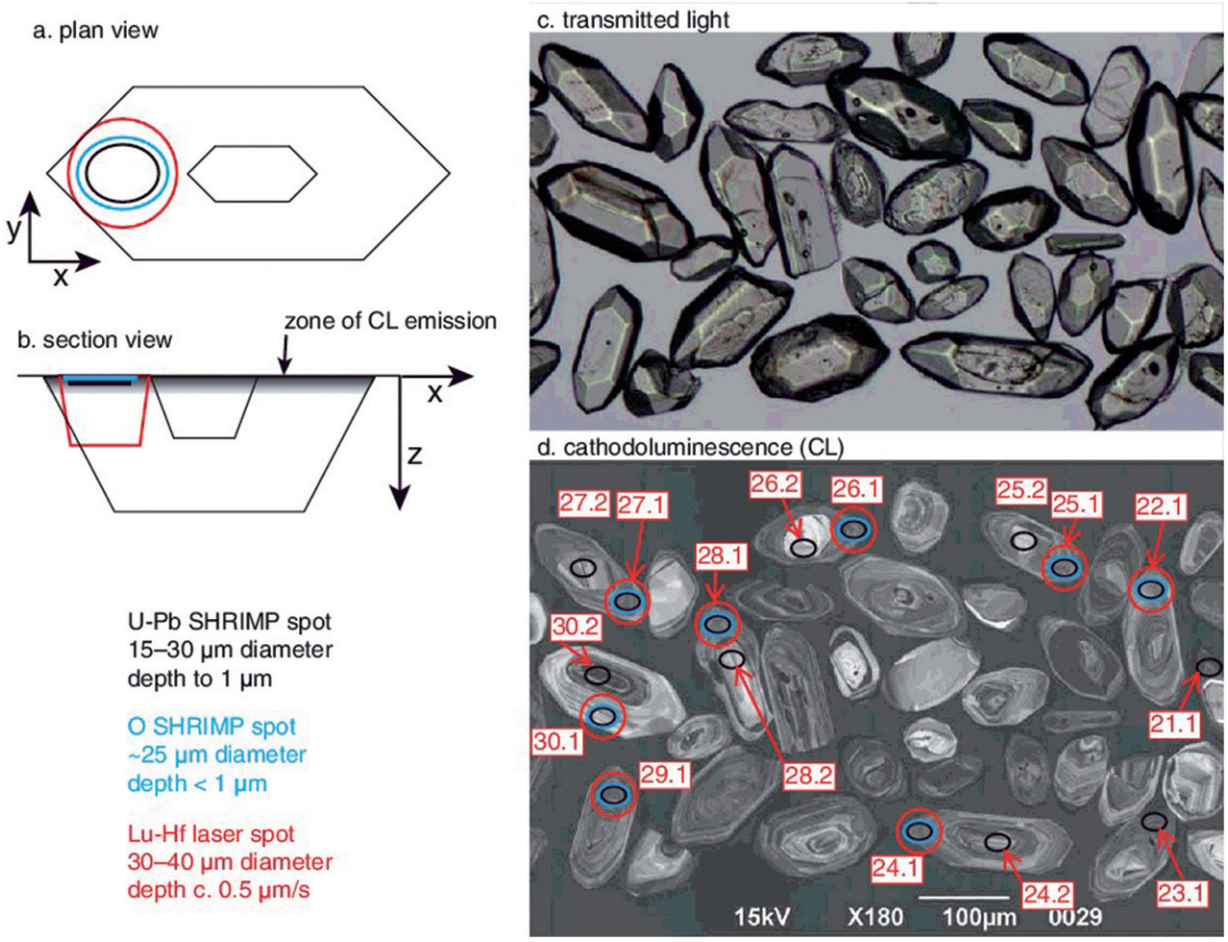

Figure 3. Illustrations of the difference in size between U–Pb (black), O (blue) and Lu–Hf (red) analytical spots, in (a) plan view, and (b) cross-sectional view. Typical zircons from the sample of Brewarrina Granite (2002535) are shown under (c) transmitted light and (d) cathodoluminescence (CL) imagery. CL reveals a much higher amount of internal complexity, but only penetrates the top 1 to 2 µm of the zircon surface, much shallower than a typical LA-ICP-MS analysis.

LA-MC-ICPMS hafnium isotope analyses of the zircons were carried out (after ion microprobe $^{18}O/^{16}O$ analyses) using a 193 nm excimer laser-based HELEX ablation system equipped with a Neptune multiple-collector inductively coupled plasma mass spectrometer described in Eggins *et al.* (2005) and Wang, Campbell, Allen, Williams, and Eggins (2009). Data were reduced offline using the software package Iolite (Hellstrom, Paton, Woodhead, & Hergt, 2008; Paton *et al.*, 2010; Paton, Hellstrom, Paul, Woodhead, & Hergt, 2011). The analyses were calibrated with the standard zircons 91500, FC1, Mud Tank, QGNG, Monastery and Plešovice (Sláma *et al.*, 2008; Wiedenbeck *et al.*, 1995; Woodhead & Hergt, 2005; Woodhead, Hergt, Shelley, Eggins, & Kemp, 2004). The nominal laser spot size was 31–41 µm, with a repetition rate of 5 Hz or 7 Hz, and ablation time was up to 60 s; laser ablation of this duration commonly resulted in excavation of a vertical hole through the entire mounted, polished zircon and into the underlying epoxy. Initial epsilon hafnium values, εHf_t, were calculated using a ^{176}Lu decay constant of 1.865×10^{-11} yr^{-1} (Scherer, Münker, & Mezger, 2001), and values of $^{176}Lu/^{177}Hf = 0.0332$, $^{176}Hf/^{177}Hf = 0.282772$ for CHUR (Blichert-Toft & Albarède, 1997). The accepted $^{176}Hf/^{177}Hf$ reference values for zircon standards used in this study are from Woodhead and Hergt (2005) and Sláma *et al.* (2008).

Lu–Hf results in the literature are commonly presented as individual spot analyses, with the sole source of uncertainty originating from the uncertainty on the analytical measurement. To properly assess a null-hypothesis that zircon from magmatic rocks represent a single population, we have expanded the Hf spot uncertainty by also incorporating the uncertainty on co-analysed reference materials, as is typically done with SHRIMP U–Pb isotope analyses.

Hf isotope analyses of some samples grouped within statistical uncertainty, and so Hf results from these samples were treated as a single population. We rejected any Hf isotope analyses with $2SE(^{176}Hf/^{177}Hf_m) > 0.000200$. This mostly arose owing to insufficient integration time during analysis, but where analysis time was sufficient, the high uncertainty was most likely due to isotopic heterogeneity or analysis of multiple domains.

O isotope analyses are more statistically dispersed than Hf-analyses in all samples. The significance of dispersion in the oxygen isotopes from these samples cannot be conclusively determined from this dataset. No images were recorded of the

grains post O isotope and prior to Hf isotope analysis so it is not possible to determine whether outliers in the O isotope data could be due to suboptimal spot placement during SHRIMP O isotope analysis. The quality of SHRIMP O isotope analysis is also highly sensitive to mount surface topography (Ickert *et al*., 2008). Mount degradation may affect O-isotope systematics. The epoxy mounts originally prepared for U–Pb SHRIMP analysis were revisited for O SHRIMP isotope analysis from 16 months (mount GA6273) to 10 years (mount Z4804) after initial preparation.

Diffusion experiments demonstrate that oxygen (Watson & Cherniak, 1997) diffuses much more readily from zircon than Pb (Cherniak & Watson, 2001), U, Th and Hf (Cherniak, Hanchar, & Watson, 1997). It is therefore possible for geological processes to disturb oxygen isotope distribution in zircon post-crystallisation, with little effect on Pb, U, Th or Hf systematics (Watson & Cherniak, 1997). For this reason, it is not possible to rule out post-crystallisation factors as a source of the dispersion in the $\delta^{18}O$ values.

Owing to the difficulties in assessing whether the scatter in $\delta^{18}O$ values was due to geological (syn- or post-crystallisation) or analytical causes, only gross outliers or those that were also outliers in Hf isotope analysis for the corresponding spot were excluded from consideration.

A detailed description of the full statistical treatment of O and Hf isotope analyses is provided in the Supplementary Papers (Appendix A).

Results

Magmatic rocks were chosen to represent regions both proximal and distal to the LTBS (Figure 2). We analysed samples from both the Thomson and the Lachlan orogens to determine whether their isotopic signatures are different. We also analysed samples east–west along the interpreted extent of the LTBS. A combination of 13 outcrop and 12 drill-core samples were utilised in this study. We focussed solely on samples previously dated by SHRIMP, which provided a library of samples for which non-destructive U–Pb isotope analyses were performed. This also allowed us to select samples largely within a 440–410 Ma time window, to minimise temporal effects and maximise the ability to interpret results within a spatial framework. A complete list of samples and their locations is provided in Table 1, and the O and Hf results are plotted in Figure 4. Below, we provide an overview of the isotopic results by spatial domain.

Albury-Bega Terrane samples

The most southerly of the sample groups, these magmatic rocks outcrop on the Nymagee 1:250 000 map sheet, in the Albury-Bega Terrane (Glen *et al*., 2009) of the central Lachlan Orogen (Figure 2). The Albury-Bega Terrane is characterised by extensive and monotonous Lower to Middle Ordovician turbidite sequences overlain by Upper Ordovician black shale-dominated sequences (Glen *et al*., 2009). The northern section of the western Albury-Bega Terrane is faulted against the northwest component of the Lachlan Orogen to the west along the Boothergandra Fault, and against the Hermidale Terrane (Glen *et al*., 2009) to the east along the Rookery Fault System (Figure 2). The northwest Albury-Bega Terrane was extensively intruded at 430–410 Ma (e.g. Black, 2007; Bodorkos *et al*., 2015; Chisholm, Blevin, Downes, & Simpson, 2014; Downes *et al*., 2016; Isaacs, 2000; Norman, 2004; Spandler, 1998).

We analysed four samples from this region: the S-type 427.2 ± 2.4 Ma Erimeran Granite (Black, 2007), the A-type 420.0 ± 2.5 Ma Boolahbone Granite (Black, 2007; Blevin & Jones, 2004), the S-type 425.7 ± 2.4 Ma Thule Granite (Chisholm *et al*., 2014) and the S-type 422.8 ± 2.6 Ma Mount Halfway Volcanics (Chisholm *et al*., 2014), the only volcanic sample in this study.

Erimeran Granite

Black (2007) documented SHRIMP U–Pb isotope analyses of this sample of Erimeran Granite (1925341). Twenty-one analyses were performed on 21 zircons. Fifteen of these analyses group to form a magmatic crystallisation age of 427.2 ± 2.4 Ma. The remainder were excluded owing to Pb loss (four analyses) and instrumental instability (two analyses).

Thirteen O isotope analyses were performed on 10 magmatic zircons (Figure 4a). Excluding one outlier, which intersected a visually damaged central region of a grain, the remaining 12 analyses range from $\delta^{18}O = 8.22$ to 10.98‰ with a weighted mean of 9.39 ± 0.56‰ (95% CI), an arithmetic mean of 9.37 ± 1.71‰ (2SD) and scatter beyond analytical uncertainty (MSWD = 12, $p = 0.000$).

Thirteen Hf isotope analyses were performed on nine magmatic zircons (Figure 4a). Two analyses were rejected: one analysis owing to large analytical uncertainty and one because it targeted a possible inherited core. The remaining 11 analyses range from $\varepsilon Hf_t = 0.282266$ to 0.282374 and form a statistically coherent weighted mean $^{176}Hf/^{177}Hf_{422.6\ Ma}$ of 0.282313 ± 0.000018 (95% CI, $\varepsilon Hf_{422.6\ Ma} = -6.9 \pm 0.6$, MSWD = 1.6, $p = 0.100$).

Boolahbone Granite

Black (2007) documented SHRIMP U–Pb isotope analyses of this sample of Boolahbone Granite (1925339). Twenty-six analyses were performed on 26 zircons. Fourteen of these analyses group to form a magmatic crystallisation age of 420.0 ± 2.5 Ma. Six analyses are interpreted to represent Cambrian to earliest Silurian inheritance, five are affected by Pb loss and one contains high common Pb.

Eleven O isotope analyses were performed on 11 zircon grains (Figure 4a). Excluding one outlier (also an outlier in Hf), the remaining analyses range between $\delta^{18}O = 8.08$ and 10.36‰, with a weighted mean of 9.72 ± 0.26‰ (95% CI), an arithmetic mean of 9.71 ± 0.69‰ (2SD) and scatter beyond analytical uncertainty (MSWD = 4.8, $p = 0.000$).

Twelve Hf isotope analyses were performed on 12 magmatic zircons (Figure 4a). Rejecting one spot owing to insufficient integration time, and excluding two obvious outliers,

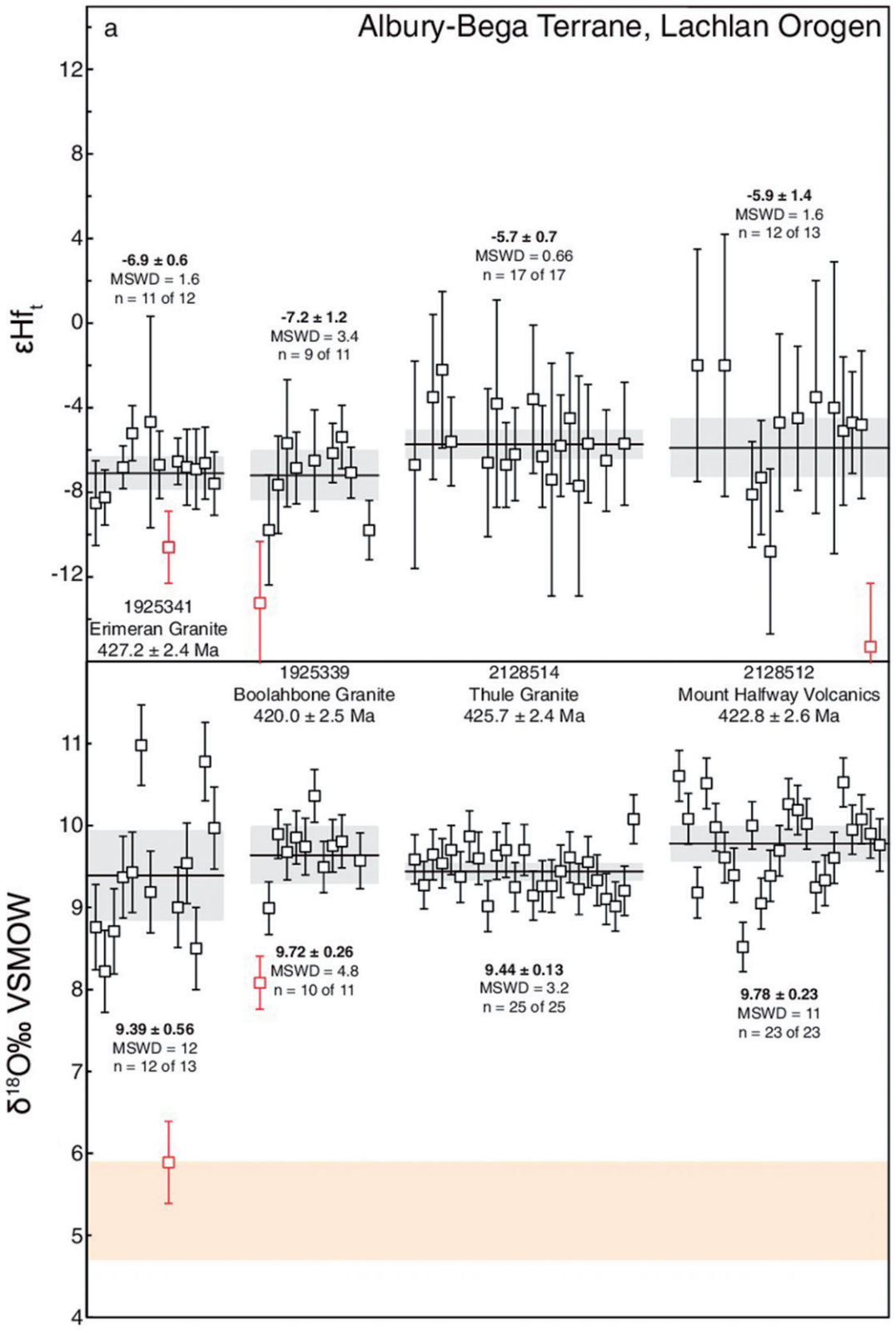

Figure 4. (a–f) Lu–Hf (upper panel) and O-isotope (lower panel) results for all samples in this study (6 pages). Spot analyses are represented by squares with 2σ error bars. Black horizontal lines represent the weighted mean of each population, and grey shaded rectangles represent the 95% confidence interval on the weighted mean. Analyses rejected from the mean are coloured red; all outliers are shown unless they are rejected due to bad analytical targets (inheritance or high common Pb), instrumental instability, insufficient integration time, or unacceptably large uncertainty [2SE ($^{176}Hf/^{177}Hf_m$) $>$ 0.000200]. Analyses are ordered by spot label, and are in the same order as the data tables presented in the Supplementary Papers. O–Hf isotope analyses that targeted the same zone on the same zircon are aligned vertically for comparison. Where there are two distinct populations in the same sample, the subordinate population is coloured blue. In the O-isotope plots, the mantle-like window (5.3 ± 0.6‰, 2SD; Valley, 2005) is shown as an orange band.

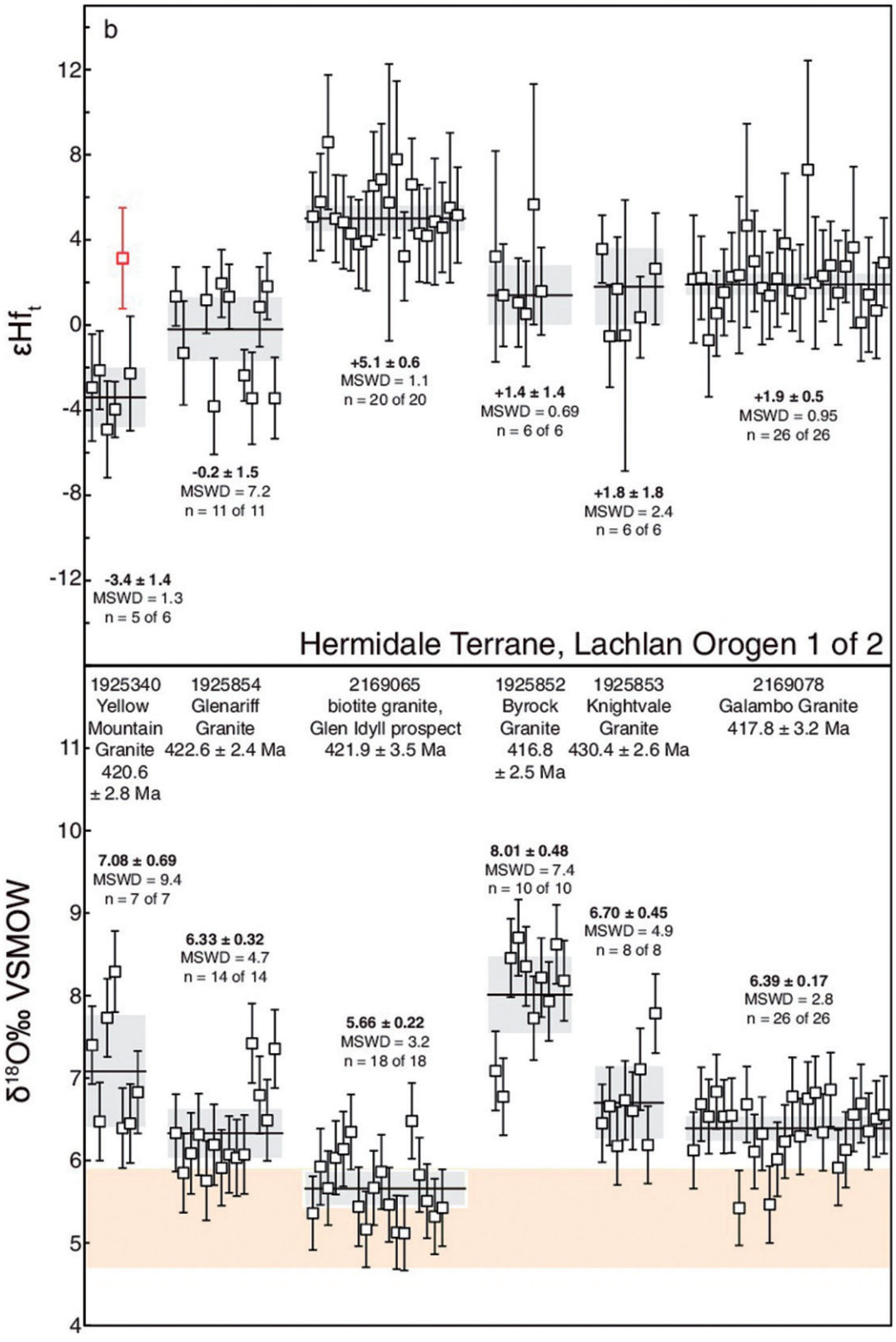

Figure 4. (*Continued*).

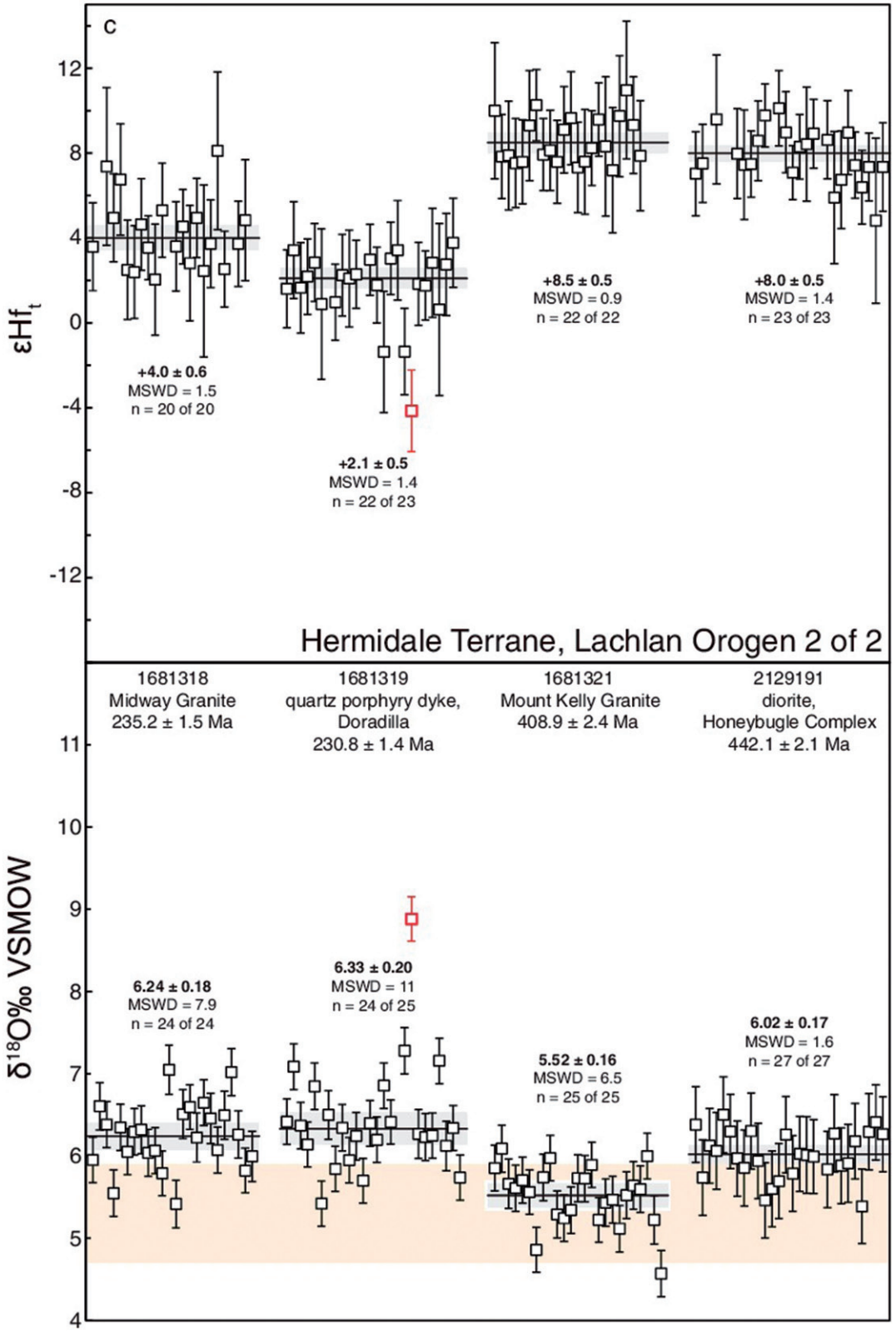

Figure 4. (*Continued*).

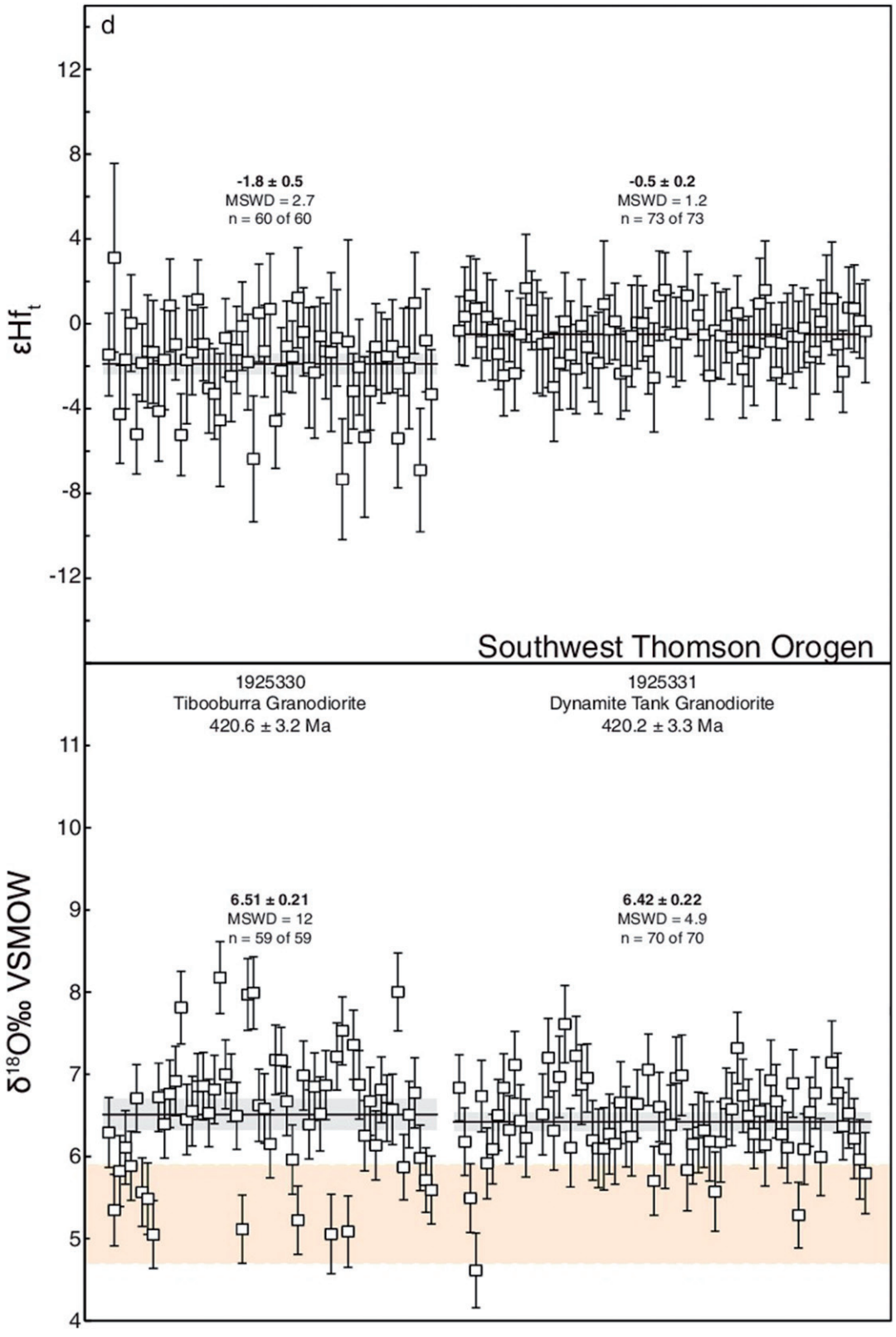

Figure 4. (*Continued*).

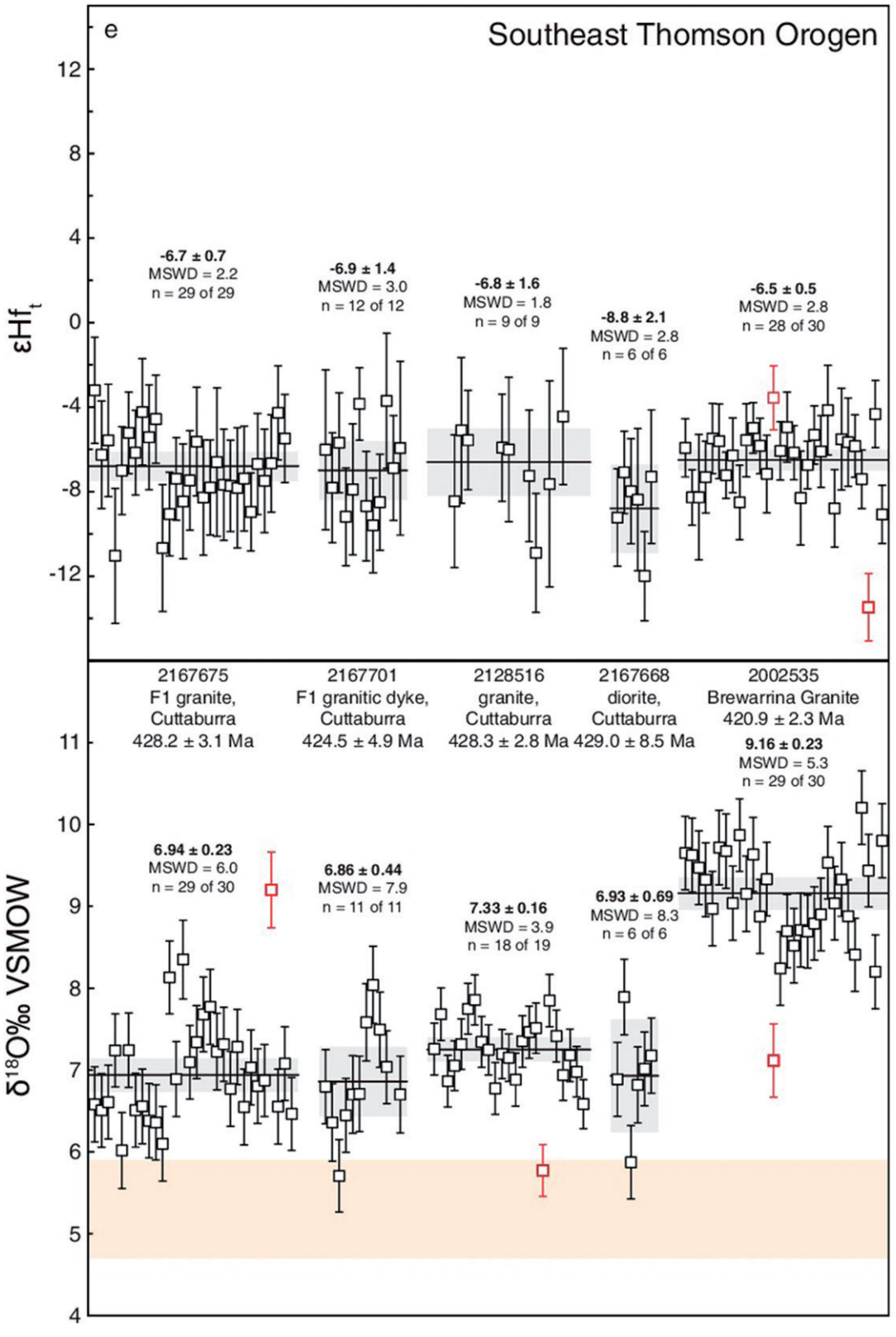

Figure 4. (*Continued*).

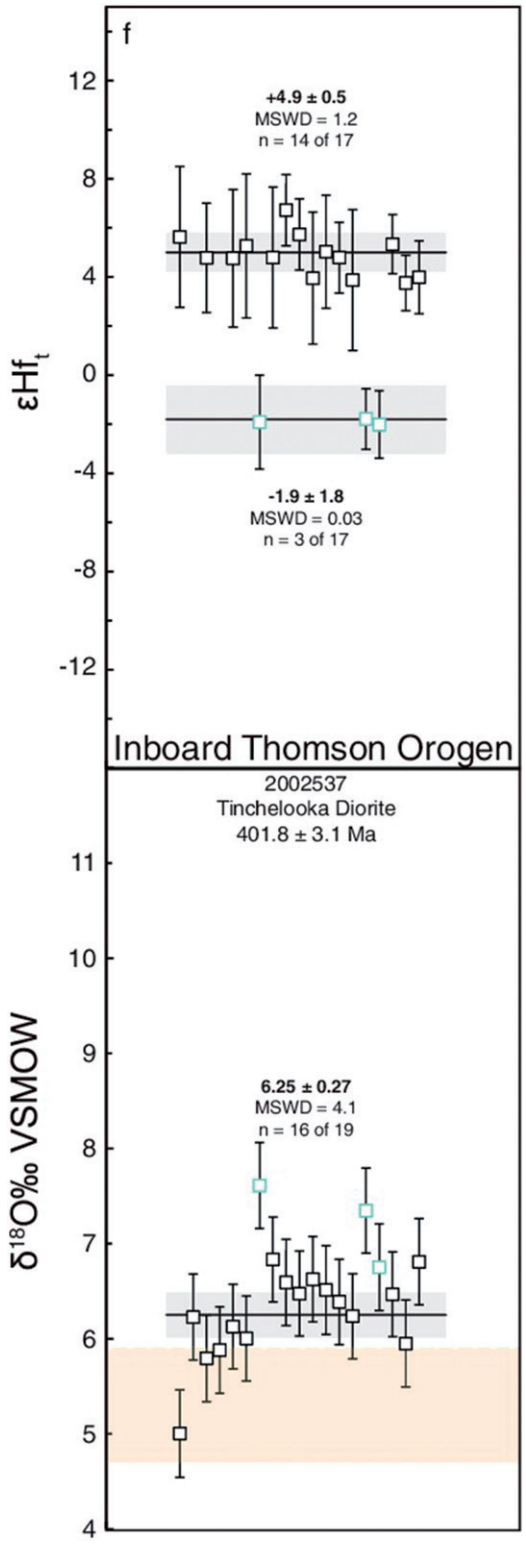

Figure 4. (*Continued*).

the remaining nine analyses range from $\varepsilon Hf_t = 0.282234$ to 0.282359 and form a population with an arithmetic mean $^{176}Hf/^{177}Hf_{420.0\ Ma}$ of 0.282318 ± 0.000092 (2SD, $\varepsilon Hf = -7.2 \pm 3.2$), a weighted mean $^{176}Hf/^{177}Hf_{420.0\ Ma}$ of 0.282308 ± 0.000034 and scatter beyond analytical uncertainty (MSWD = 3.4, $p = 0.000$).

Thule Granite

Chisholm *et al*. (2014) documented SHRIMP U–Pb isotope analyses of this sample of Thule Granite (2128514). Thirty-one analyses were performed on 29 zircons. Twenty-eight analyses group to form a magmatic crystallisation age of 425.7 ± 2.4 Ma. The remaining three analyses are attributed to inheritance.

Twenty-five O isotope analyses were performed on 25 magmatic zircons (Figure 4a). The analyses range from $\delta^{18}O =$ 9.01 to 10.08‰ (95% CI), with a weighed mean of 9.44 ± 0.13‰, an arithmetic mean of 9.44 ± 0.54‰ (2SD) and scatter beyond analytical uncertainty (MSWD = 3.2, $p = 0.000$).

Twenty-five Hf isotope analyses were performed on 25 magmatic zircons (Figure 4a). Rejecting eight analyses owing to high analytical uncertainty, the remaining 17 analyses range from $\varepsilon Hf_t = 0.282291$ to 0.282444 and form a statistically coherent population with a weighted mean $^{176}Hf/^{177}Hf_{425.7\ Ma}$ of 0.282346 ± 0.000021 (95% CI, $\varepsilon Hf_{425.7\ Ma} = -5.7 \pm 0.7$, MSWD = 0.66, $p = 0.83$).

Mount Halfway Volcanics

Chisholm *et al*. (2014) documented SHRIMP U–Pb isotope analyses of this sample of the Mount Halfway Volcanics (2128512). Thirty-three analyses were performed on 28 zircons. Twenty-three analyses group to form a magmatic crystallisation age of 422.8 ± 2.6 Ma. Seven analyses recorded inheritance and three were not considered due to instrument instability.

Twenty-three O isotope analyses were performed on 22 magmatic zircons (Figure 4a). The analyses range from $\delta^{18}O =$ 8.52 to 10.60‰ (95% CI), with a weighted mean of 9.78 ± 0.23‰, an arithmetic mean of 9.78 ± 1.03‰ (2SD) and scatter beyond analytical uncertainty (MSWD = 11, $p = 0.000$).

Twenty-three Hf isotope analyses were performed on 22 magmatic zircon grains (Figure 4a). The mounted zircons were thin and it was difficult to obtain sufficient integration times on these grains, resulting in rejecting one analysis that did not obtain any usable data and nine other grains owing to high uncertainty. Excluding one obvious outlier, the remaining 12 analyses range from $\varepsilon Hf_t = 0.282203$ to 0.282452 and form a statistically coherent weighted mean $^{176}Hf/^{177}Hf_{422.8\ Ma}$ of 0.282343 ± 0.000040 (95% CI, $\varepsilon Hf_{422.8\ Ma} = -5.9 \pm 1.4$, MSWD = 1.6, $p = 0.090$)

Hermidale Terrane samples

This region corresponds to the Hermidale Terrane as described in Glen *et al*. (2009). Like the Albury-Bega Terrane to the southwest, this domain comprises Lower to Middle Ordovician turbidite and chert sequences, but differs in the absence of Upper Ordovician units and the presence of mafic volcanic rocks (Glen *et al*., 2009). This terrane is bounded by the Rookery Fault Zone to the southwest, which separates it from the Albury-Bega Terrane, the Tullamore Fault Zone to the east,

which separates it from the Macquarie Arc, and the Little Mountain Fault–Mount Oxley Fault of the Louth-Eumarra Shear Zone to the north, which separate it from the Thomson Orogen (Figure 2). The overlying upper Silurian–Devonian Cobar Basin is intruded by multiple igneous units of mostly I-type composition.

We analysed 10 samples from this domain, all I-type in character. In the south of the Hermidale Terrane, we analysed the 420.6 ± 2.8 Ma Yellow Mountain Granite (Black, 2007). From the northern half of the Hermidale Terrane: the 422.6 ± 2.4 Ma Glenariff Granite (Black, 2007) from 'DDH1' from the Glenariff D2000 program drilled by the Department of Mineral Resources in 1996; a 421.9 ± 3.5 Ma unnamed granite (Fraser *et al*., in prep.) 21 km to the southwest of the hamlet of Gongolgon in the Glen Idyll Prospect from diamond drill core TDBTRCD002 drilled by Straits Resources Limited; the outcropping 416.8 ± 2.5 Ma Byrock Granite (Black, 2007); the 430.4 ± 2.6 Ma Knightvale Granite (Black, 2007) from diamond drill hole drilled by CRA Exploration Pty Ltd in 1978; and the 417.8 ± 3.2 Ma Galambo Granite (Fraser *et al*., in prep.) from drill hole 5064/CAC-05.5, drilled by Croesus Mining NL in 1997. Two younger granites were analysed, the 235.2 ± 1.5 Ma Midway Granite (Black, 2006), and a 230.8 ± 1.4 Ma unnamed quartz porphyry dyke (Black, 2006) to the southwest of the Midway Granite. The Midway Granite is an extremely fractionated I-type granite and is associated with Sn mineralisation at the Doradilla prospect (Blevin, 2011; Burton, Trigg, & Black, 2007). The Midway Granite and associated dyke were analysed to understand the relationship between these younger, spatially restricted magmatic rocks and the more common and widespread 430–410 Ma occurrences. We also analysed the outcropping 408.9 ± 2.4 Ma Mount Kelly Granite (Black, 2006) and the 442.1 ± 2.1 Ma Honeybugle Granite (Fraser *et al*., 2014). The Honeybugle Granite is older than the bulk of the samples in this study, but its inclusion aids with investigation of the influence of the proximal Macquarie Arc.

Yellow Mountain Granite

Black (2007) documented SHRIMP U–Pb isotope analyses of this sample of Yellow Mountain Granite (1925340). Twenty-three analyses were performed on 23 zircons. Only eight of these analyses are interpreted to represent magmatic crystallisation at 420.6 ± 2.8 Ma. The remaining 15 analyses are interpreted to represent inheritance.

Seven O isotope analyses were performed on seven magmatic zircons (Figure 4b). These analyses range from $\delta^{18}O$ = 6.39 to 8.29‰, with a weighted mean of 7.08 ± 0.69‰ (95% CI), an arithmetic mean of 7.12 ± 1.60‰ (2SD) and scatter beyond analytical uncertainty (MSWD = 9.4, $p = 0.000$).

Six Hf isotope analyses were performed on six magmatic zircons (Figure 4b). Excluding one outlier, the remaining five analyses range from $\varepsilon Hf_t = 0.282372$ to 0.082451 and form a statistically coherent population with a weighted mean $^{176}Hf/^{177}Hf_{420.6\ Ma}$ of 0.282414 ± 0.000039 ($\varepsilon Hf_{420.6\ Ma} = -3.4 \pm 1.4$, MSWD = 1.3, $p = 0.26$).

Glenariff Granite

Black (2007) documented SHRIMP U–Pb isotope analyses of this sample of Glenariff Granite (1925854). Twenty-three analyses were performed on 22 zircons. Fourteen group to form a magmatic crystallisation age of 422.6 ± 2.4 Ma. The remainder were affected by Pb loss (8) or analysed an area of core–rim overlap.

Fourteen O isotope analyses were performed on 14 magmatic zircons (Figure 4b). The analyses range from $\delta^{18}O = 5.76$ to 7.42‰, with a weighted mean of 6.33 ± 0.32‰ (95% CI), an arithmetic mean of 6.33 ± 1.04‰ (2SD) and scatter beyond analytical uncertainty (MSWD = 4.7, $p = 0.000$).

Twelve Hf isotope analyses were performed on 12 magmatic zircons grains (Figure 4b). Rejecting one analysis owing to high analytical uncertainty, the remaining 11 analyses range from $\varepsilon Hf_t = 0.282402$ to 0.282565 and form an arithmetic mean $^{176}Hf/^{177}Hf_{422.6\ Ma}$ of 0.282494 ± 0.000133 (2SD, $\varepsilon Hf_{422.6\ Ma} = -0.5 \pm 4.7$), a weighted mean $^{176}Hf/^{177}Hf_{422.6\ Ma}$ of 0.282504 ± 0.000042 (95% CI), and scatter beyond analytical uncertainty (MSWD = 7.2, $p = 0.000$).

Unnamed biotite granite, Glen Idyll Prospect

Fraser *et al*. (in prep.) documented SHRIMP U–Pb isotope analyses of this sample of unnamed biotite granite at the Glen Idyll Prospect (2169065). Twenty-eight analyses were performed on 28 zircons. Twenty-one analyses group to form a magmatic crystallisation age of 421.9 ± 3.5 Ma. The remaining seven analyses had high common Pb.

Eighteen O isotope analyses were performed on 18 magmatic zircons (Figure 4b). These analyses range from $\delta^{18}O = 5.12$ to 6.48‰, with a weighted mean $\delta^{18}O$ of 5.66 ± 0.22‰ (95% CI), an arithmetic mean $\delta^{18}O$ of 5.66 ± 0.82‰ (2SD) and scatter beyond analytical uncertainty (MSWD = 3.2, $p = 0.000$).

Twenty Hf isotope analyses were performed on 20 magmatic zircons (Figure 4b). These analyses range from $\varepsilon Hf_t = 0.282603$ to 0.282755 and form a statistically coherent weighted mean $^{176}Hf/^{177}Hf_{421.9\ Ma}$ of 0.282654 ± 0.000017 (95% CI, $\varepsilon Hf_{421.9\ Ma} = +5.1 \pm 0.6$, MSWD = 1.1, $p = 0.35$).

Byrock Granite

Black (2007) documented SHRIMP U–Pb isotope analyses of this sample of Byrock Granite (1925852), where it was referred to as 'Westella Granite.' Twenty-three analyses were performed on 23 zircons. Thirteen analyses group to form a magmatic crystallisation age of 416.8 ± 2.5 Ma. The remaining analyses were attributed to inheritance (5 spots) and radiogenic Pb loss (5 spots).

Ten O isotope analyses were performed on 10 magmatic zircons (Figure 4b). The analyses range from $\delta^{18}O = 6.77$ to 8.70‰, with a weighted mean of 8.01 ± 0.48‰ (95% CI), an arithmetic mean of 8.00 ± 1.28‰ (2SD) and scatter beyond analytical uncertainty (MSWD = 7.4, $p = 0.000$).

Nine Hf isotope analyses were performed on nine magmatic zircon grains (Figure 4b). Rejecting three analyses owing to high analytical uncertainty, the remaining six analyses range from $\varepsilon Hf_t = 0.282528$ to 0.282673 and form a

statistically coherent population with a weighted mean $^{176}Hf/^{177}Hf_{416.8\ Ma}$ of 0.282553 ± 0.000039 ($\varepsilon Hf_{416.8\ Ma}$ = +1.4 ± 1.4, MSWD = 0.69, p = 0.63).

Knightvale Granite

Black (2007) documented SHRIMP U–Pb isotope analyses of this sample of Knightvale Granite (1925853). Twenty-two analyses were performed on 22 zircons. Ten group to form a magmatic crystallisation age of 430.4 ± 2.6 Ma. Eleven targeted inheritance, and one was rejected because it was situated on a crack.

Eight O isotope analyses were performed on eight magmatic zircons (Figure 4b). The analyses range from $\delta^{18}O$ = 6.18 to 7.78‰, with a weighted mean of 6.70 ± 0.45‰ (95% CI), an arithmetic mean of 6.71 ± 1.05‰ (2SD) and scatter beyond analytical uncertainty (MSWD = 4.9, p = 0.000).

Eight Hf isotope analyses were performed on eight magmatic zircon grains (Figure 4b). We rejected one analysis because it did not produce any usable data, and another because of high analytical uncertainty. The remaining six analyses range from εHf_t = 0.282490 to 0.282605 and form an arithmetic mean $^{176}Hf/^{177}Hf_m$ of 0.282577 ± 0.000087 (2SD, $\varepsilon Hf_{430.4\ Ma}$ = +1.2 ± 3.4), a weighted mean $^{176}Hf/^{177}Hf_m$ of 0.282554 ± 0.000052 and scatter beyond analytical uncertainty (MSWD = 2.4, p = 0.037).

Galambo Granite

Fraser *et al*. (in prep.) documented SHRIMP U–Pb isotope analyses of this sample of Galambo Granite (2169078). Thirty-two analyses were performed on 32 zircons. Twenty-six analyses grouped to form a magmatic crystallisation age of 417.8 ± 3.2 Ma. Five analyses had high common Pb, and one was affected by Pb loss.

Twenty-six O isotope analyses were performed on 26 magmatic zircons (Figure 4b). These analyses range from $\delta^{18}O$ = 5.42 to 6.86‰, with a weighted mean $\delta^{18}O$ of 6.39 ± 0.17‰ (95% CI), an arithmetic mean $\delta^{18}O$ of 6.39 ± 0.77‰ (2SD) and scatter beyond analytical uncertainty (MSWD = 2.8, p = 0.000).

Twenty-six Hf isotope analyses were performed on 26 magmatic zircons (Figure 4b). These analyses range from εHf_t = 0.282494 to 0.282720 and form a statistically coherent weighted mean $^{176}Hf/^{177}Hf_{417.8\ Ma}$ of 0.282567 ± 0.000014 (95% CI, $\varepsilon Hf_{418\ Ma}$ = +1.9 ± 0.5, MSWD = 0.95, p = 0.53).

Midway Granite

Black (2006) documented SHRIMP U–Pb isotope analyses of this sample of Midway Granite (1681318). Thirty-eight analyses were performed on 38 zircons. Thirty-one analyses grouped to form a magmatic crystallisation age of 235.2 ± 1.5 Ma. Six other spots recorded Neoproterozoic to Ordovician inheritance. A single analysis was affected by Pb loss.

Twenty-four O isotope analyses were performed on 24 magmatic zircon grains (Figure 4c). The analyses range from $\delta^{18}O$ = 5.42 to 7.05‰, with a weighted mean of 6.24 ± 0.18‰ (95% CI), an arithmetic mean of 6.25 ± 0.81‰ (2SD) and scatter beyond analytical uncertainty (MSWD = 7.9, p = 0.000).

Twenty-four Hf isotope analyses were performed on 24 magmatic zircon grains (Figure 4c). Rejecting four analyses owing to high analytical uncertainty, the remaining 20 analyses range from εHf_t = 0.282684 to 0.282855 and give a statistically coherent weighted mean $^{176}Hf/^{177}Hf_{235.1\ Ma}$ of 0.282739 ± 0.000018 (95% CI, $\varepsilon Hf_{235.1\ Ma}$ = +4.0 ± 0.6, MSWD = 1.5, p = 0.088).

Unnamed quartz porphyry dyke, Doradilla

Black (2006) documented SHRIMP U–Pb isotope analyses of this sample of unnamed quartz porphyry dyke (1681319), which occurs as part of a dyke swarm near the Midway Granite. Thirty-eight analyses were performed on 38 zircons. Thirty-four of these spots have an age range of 236–224 Ma, and form a magmatic crystallisation age of 230.8 ± 1.4 Ma. One spot recorded earliest Triassic inheritance, and three spots are interpreted to have been affected by loss of radiogenic Pb.

Twenty-five O isotope analyses were performed on 25 zircon grains (Figure 4c). Rejecting one outlier as it is also an outlier in Hf, the remaining 24 analyses range from $\delta^{18}O$ = 5.42 to 7.28‰, with a weighted mean of 6.33 ± 0.20‰ (95% CI), an arithmetic mean of 6.34 ± 0.92‰ (2SD) and scatter outside analytical uncertainty (MSWD = 11, p = 0.000).

Twenty-five Hf isotope analyses were performed on 25 magmatic zircon grains (Figure 4c). Rejecting two analyses because of high analytical uncertainty, in addition to the removal of one outlier (also an outlier in O isotope analysis), the remaining analyses range from εHf_t = 0.282590 to 0.282736 and form a statistically coherent weighted mean $^{176}Hf/^{177}Hf_{230.7\ Ma}$ of 0.282687 ± 0.000015 ($\varepsilon Hf_{230.7\ Ma}$ = +2.1 ± 0.5, MSWD = 1.4, p = 0.102).

Mount Kelly Granite

Black (2006) documented SHRIMP U–Pb isotope analyses of this sample of Mount Kelly Granite (1681321). Thirty-eight analyses were performed on 38 zircons. Thirty-seven of these analyses range in age from 421 to 398 Ma and group to form a magmatic crystallisation age of 408.9 ± 2.4 Ma. The remaining spot was affected by Pb loss.

Twenty-five O isotope analyses were performed on 25 magmatic zircon grains (Figure 4c). These analyses range between $\delta^{18}O$ = 4.57 and 6.09‰, with a weighted mean of 5.52 ± 0.16‰ (95% CI), an arithmetic mean of 5.52 ± 0.72‰ (2SD), and scatter outside analytical uncertainty (MSWD = 6.5, p = 0.000).

Twenty-five Hf isotope analyses were performed on 25 magmatic zircon grains (Figure 4c). Rejecting the final three analyses owing to possible analytical instability, the remaining 22 analyses range from εHf_t = 0.282722 to 0.282828 and form a statistically coherent group with a weighted mean $^{176}Hf/^{177}Hf_{408.9\ Ma}$ of 0.282759 ± 0.000014 (95% CI, $\varepsilon Hf_{408.9\ Ma}$ = +8.5 ± 0.5, MSWD = 0.90, p = 0.59).

Honeybugle Complex diorite

Fraser *et al*. (2014) documented SHRIMP U–Pb isotope analyses of this sample of Honeybugle Complex diorite (2129191). Twenty-eight analyses were performed on 27 zircon grains. Twenty-seven analyses group to form a magmatic crystallisation age of 442.1 ± 2.1 Ma. The remaining analysis was not considered owing to high common Pb.

Twenty-eight O isotope analyses were performed on 27 magmatic zircons (Figure 4c). Rejecting one analysis as it targeted a region identified to have high common Pb, the remaining 27 analyses range from $\delta^{18}O = 5.39$ to 6.50‰, with a weighted mean of 6.02 ± 0.17‰ (95% CI), an arithmetic mean of 6.02 ± 0.58‰ (2SD) and scatter beyond analytical uncertainty (MSWD = 1.6, $p = 0.026$).

Twenty-eight Hf isotope analyses were performed on 27 magmatic grains (Figure 4c). Rejecting four analyses owing to high analytical uncertainty and one that targeted a region identified to have high common Pb, the remaining 23 analyses range from $\varepsilon Hf_t = 0.282633$ to 0.282783 and form a statistically coherent population with a weighted mean $^{176}Hf/^{177}Hf_{442.1\ Ma}$ of 0.282723 ± 0.000014 (95% CI, $\varepsilon Hf_{442.1\ Ma} = +8.0 \pm 0.5$, MSWD = 1.4, $p = 0.09$).

Southwest Thomson Orogen samples

The surface of the southwest Thomson Orogen is largely covered by unconsolidated sediments, however there are three exposures of upper Cambrian to Lower Ordovician sediments of the Warratta Group on or near the boundary of the Thomson Orogen, separated from the Koonenberry Belt by the Olepoloko Fault (Figure 2; Greenfield *et al*., 2010). The Warratta Group is interpreted to have an extensive sub-surface extent (Purdy *et al*., 2018). A gravity high is observed under the Warratta Group, interpreted to be magmatic underplating, and the surface expression of this geophysical feature is interpreted to be the Tibooburra Suite, which intrudes parts of the Warratta Group (Greenfield *et al*., 2010). Geochemistry of rocks from the Tibooburra Suite suggests they have a heterogeneous mantle source, with variable amounts of crustal contamination (Greenfield *et al*., 2010). The Koonenberry Belt hosts the lower–middle Cambrian Mount Wright Arc, interpreted to be volcanic arc system, oriented with the back-arc to the southwest (Greenfield *et al*., 2011).

We analysed two samples from the Tibooburra Suite: the 420.5 ± 3.2 Ma I-type Tibooburra Granodiorite (Black, 2007), and a 420.2 ± 3.3 Ma I-type hornblende diorite of the Dynamite Tank Granodiorite (Black, 2007). Siégel (2015) reports the U–Pb, O and Hf isotopic data from the 419.0 ± 2.7 Ma S-type Wolgolla Granite from the base of petroleum exploration well WOLGOLLA 1 (drilled by Delhi in 1973), which is also relevant to this study.

Tibooburra Granodiorite

Black (2007) documented SHRIMP U–Pb isotope analyses of this sample of the Tibooburra Granodiorite (1925330). Eighty-three analyses were performed over several analytical sessions. Fifty-eight analyses group to form a magmatic crystallisation age of 420.5 ± 3.2 Ma. A further 19 analyses are interpreted to also represent magmatic crystallisation but are from an aberrant SHRIMP session. A single analysis was attributed to inheritance, four were interpreted to have been affected by Pb loss, and a single analysis contained high common Pb.

Fifty-nine O isotope analyses were performed on 58 magmatic zircons (Figure 4d). These analyses range between $\delta^{18}O = 5.05$ and 8.18‰, with a weighted mean of 6.51 ± 0.21‰ (95% CI), an arithmetic mean of 6.51 ± 1.51‰ (2SD), and scatter beyond analytical uncertainty (MSWD = 12, $p = 0.000$).

Sixty-eight Hf isotope analyses were performed on 66 magmatic zircon grains (Figure 4d). Excluding six analyses that yielded no usable data, and one other owing to high analytical uncertainty, the remaining 60 analyses range from $\varepsilon Hf_t = 0.282305$ to 0.282600 and combine to form an arithmetic mean $^{176}Hf/^{177}Hf_{420.6\ Ma}$ of 0.282466 ± 0.000117 (2SD, $\varepsilon Hf_{420.6\ Ma} = -1.9 \pm 4.1$), a weighted mean $^{176}Hf/^{177}Hf_{420.6\ Ma}$ of 0.282460 ± 0.000014 and scatter beyond analytical uncertainty (MSWD = 2.7, $p = 0.000$).

Dynamite Tank Granodiorite

Black (2007) documented SHRIMP U–Pb isotope analyses of this sample of hornblende diorite (1925331), interpreted to be a marginal phase of the Dynamite Tank Granodiorite (Greenfield *et al*., 2010) near Tibooburra. Eighty-two analyses were performed over several analytical sessions. Fifty-eight analyses group to form a magmatic crystallisation age of 420.2 ± 3.3 Ma. A further 18 analyses are interpreted to represent magmatic crystallisation but are from an aberrant SHRIMP session. Four analyses were interpreted to represent inheritance, and two analyses were young outliers to the magmatic population.

Seventy O isotope analyses were performed on 70 magmatic zircons (Figure 4d). These analyses range from $\delta^{18}O = 5.29$ to 7.61‰, with a weighted mean of 6.42 ± 0.22‰ (95% CI), an arithmetic mean of 6.42 ± 1.00‰ (2SD), and scatter beyond analytical uncertainty (MSWD = 4.9, $p = 0.000$).

Seventy-four Hf isotope analyses were performed on 72 magmatic zircon grains (Figure 4d). These analyses range from $\varepsilon Hf_t = 0.282428$ to 0.282560 and form a statistically coherent weighted mean $^{176}Hf/^{177}Hf_{420.2\ Ma}$ of 0.282498 ± 0.000008 (95% CI, $\varepsilon Hf_{420.2\ Ma} = -0.5 \pm 0.2$, MSWD = 1.2, $p = 0.11$).

Southeast Thomson Orogen samples

Surface exposure of granite is sparse in the southeast Thomson Orogen. We investigated several samples from within a few kilometres to the north of the eastern Olepoloko Fault, the Little Mountain Fault and the Mount Oxley Fault (Figure 2).

We analysed four plutonic rocks from drill core in the Cuttaburra region: a 428.2 ± 3.1 Ma medium-grained, biotite-rich I-type granite (Armistead & Fraser, 2015) from drill hole F1DD02 (Thomson Resources, drilled in 2013), a 424.5 ±

4.9 Ma leucocratic granitic I-type dyke (Armistead & Fraser, 2015) from drill hole F1DD01 (Thomson Resources, drilled in 2013), a 428.3 ± 2.8 Ma I-type granodiorite named 'Cuttaburra granite' (Chisholm *et al*., 2014) from drill hole CUTAD01 (Thomson Resources, drilled in 2011), and a 429.0 ± 8.5 Ma biotite-rich S-type quartz diorite (Armistead & Fraser, 2015) from drill hole CUTACD02 (Thomson Resources, drilled in 2011). Armistead *et al*. (2017) performed petrographic and geochemical classification of these rocks. Although these rocks were described as geochemically transitional between S-and I-type, the researchers acknowledged that some samples were intensely hydrothermally altered. Petrography of the S-type diorite from CUT1CD02 revealed 2–3 mm domains suggestive of xenoliths of sedimentary rock, suggesting that the bulk-rock geochemistry of this rock may be affected by country-rock contamination (Armistead *et al*., 2017). The $\delta^{18}O$ values from these samples are more suggestive of all of these samples being I-type (see below).

We also analysed the S-type 420.9 ± 2.3 Ma Brewarrina Granite (Bodorkos *et al*., 2013) farther to the east, to the north of the Mount Bendemeer Fault.

Unnamed granite, F1 prospect

Armistead and Fraser (2015) documented SHRIMP U–Pb isotope analyses of this sample of unnamed granite (2167675) from the F1 prospect. Forty-two analyses were performed on 40 zircon grains. Thirty-one analyses group to form a magmatic crystallisation age of 428.2 ± 3.1 Ma. Ten other analyses targeted inheritance, and one was interpreted to have been affected by Pb loss.

Thirty O isotope analyses were performed on 30 magmatic zircons (Figure 4e). Excluding one spot as an outlier that may have been situated on an inclusion, the remainder range from $\delta^{18}O = 6.02$ to 8.35‰, with a weighted mean of 6.94 ± 0.23‰ (95% CI), an arithmetic mean of 6.94 ± 1.13‰ (2SD) and scatter beyond analytical uncertainty (MSWD = 6.0, $p = 0.000$).

Thirty Hf isotope analyses were performed on 30 magmatic zircon grains (Figure 4e). Rejecting one spot owing to large analytical uncertainty, the remaining 29 analyses range from $\varepsilon Hf_t = 0.282196$ to 0.282417 and yield an arithmetic mean $^{176}Hf/^{177}Hf_{428.2\ Ma}$ of 0.282312 ± 0.000103 (2SD; $\varepsilon Hf_{428.2\ Ma} = -6.8 \pm 3.7$), a weighted mean $^{176}Hf/^{177}Hf_{428.2\ Ma}$ of 0.282315 ± 0.000019, with scatter outside analytical uncertainty (MSWD = 2.2, $p = 0.000$).

Unnamed granitic dyke, F1 prospect

Armistead and Fraser (2015) documented SHRIMP U–Pb isotope analyses of this sample of unnamed granitic dyke (2167701) from the F1 prospect. Twenty-seven analyses were performed on 22 zircon grains. Thirteen of the analyses group to form a magmatic crystallisation age of 424.5 ± 4.9 Ma. The remaining analyses represent inheritance.

Eleven O isotope analyses were performed on 10 magmatic zircons (Figure 4e). These analyses ranged between $\delta^{18}O = 5.71$ and 8.04‰, with a weighted mean of 6.86 ± 0.44‰ (95% CI), an arithmetic mean of 6.87 ± 1.23‰ (2SD) and scatter beyond analytical uncertainty (MSWD = 7.9, $p = 0.000$).

Twelve Hf isotope analyses were performed on 10 magmatic zircons (Figure 4e). These analyses range from $\varepsilon Hf_t = 0.282239$ to 0.282405 and form an arithmetic mean $^{176}Hf/^{177}Hf_{424.5\ Ma}$ of 0.282313 ± 0.0000111 (2SD, $\varepsilon Hf_{424.5\ Ma} = -6.9 \pm 3.9$), a weighted mean $^{176}Hf/^{177}Hf_{424.5\ Ma}$ of 0.282314 ± 0.000039 and scatter beyond analytical uncertainty (MSWD = 3.0, $p = 0.001$).

Unnamed granite, Cuttaburra

Chisholm *et al*. (2014) documented SHRIMP U–Pb isotope analyses of this sample of unnamed granite (2128516) near Cuttaburra. Twenty-three analyses were performed on 21 zircons. Nineteen analyses group to form a magmatic crystallisation age of 428.3 ± 2.8 Ma. The remaining four analyses are attributed to inheritance.

Twenty-three O isotope analyses were performed on 21 magmatic zircons (Figure 4e). Excluding one outlier, and four spots located on inherited regions, the remaining 18 analyses range from $\delta^{18}O = 6.87$ to 7.86‰, with a weighted mean of 7.33 ± 0.16‰ (95% CI), an arithmetic mean of 7.33 ± 0.62‰ (2SD) and scatter beyond analytical uncertainty (MSWD = 3.9, $p = 0.000$).

Twenty-three Hf isotope analyses were performed on 21 zircons (Figure 4e). Many of the mounted zircons were thin, and it was difficult to obtain sufficient integration time. Rejecting 10 grains owing to high analytical uncertainty, and four because they targeted inherited regions of grains, the remaining nine analyses range from $\varepsilon Hf_t = 0.282198$ to 0.282380 and form a statistically coherent population with a weighted mean $^{176}Hf/^{177}Hf_{428.3\ Ma}$ of 0.282314 ± 0.000029 (95% CI, $\varepsilon Hf_{428.3\ Ma} = -6.8 \pm 1.6$, MSWD = 1.8, $p = 0.067$).

Unnamed quartz diorite, Cuttaburra

Armistead and Fraser (2015) documented SHRIMP U–Pb isotope analyses of this sample of unnamed quartz diorite (2167668) from drill hole CUTACD02. Forty-two analyses were performed on 41 zircon grains. Six of these analyses group to form a magmatic crystallisation age of 429.0 ± 8.5 Ma. Twenty-five of the remaining analyses represent inheritance, and 11 others were not considered owing to high common Pb.

Six O isotope analyses were performed on six magmatic zircons (Figure 4e). The analyses range from $\delta^{18}O = 5.87$ to 7.89‰, with a weighted mean of 6.93 ± 0.69‰ (95% CI), an arithmetic mean of 6.94 ± 1.30‰ (2SD) and scatter beyond analytical uncertainty (MSWD = 8.3, $p = 0.000$).

Six Hf isotope analyses were performed on six magmatic zircon grains (Figure 4e). The analyses range from $\varepsilon Hf_t = 0.282168$ to 0.282307 and give an arithmetic mean $^{176}Hf/^{177}Hf_{429.0\ Ma}$ of 0.282262 ± 0.0000102 (2SD, $\varepsilon Hf_{429.0\ Ma} = -8.6 \pm 3.6$), a weighted mean $^{176}Hf/_{177}Hf_{429.0\ Ma}$ of 0.282258 ± 0.000060, and scatter beyond analytical uncertainty (MSWD = 2.8, $p = 0.017$).

Brewarrina Granite

Bodorkos *et al*. (2013) documented SHRIMP U–Pb isotope analyses of this sample of the Brewarrina Granite (2002535). Forty analyses were conducted on 34 zircon grains. Thirty-two group to give a magmatic crystallisation age of 420.9 ± 2.3 Ma. Seven analyses in the range 1729–466 Ma were interpreted as inherited, and one analysis was interpreted to have been affected by Pb loss.

Thirty O isotope analyses were performed on 30 magmatic zircons (Figure 4e). Excluding one outlier, also showing possible disturbance in Hf, the remaining 29 analyses range from $\delta^{18}O$ = 8.20 to 10.20‰, with a weighted mean of 9.16 ± 0.23‰ (95% CI), an arithmetic mean of 9.16 ± 1.03‰ (2SD) and scatter beyond analytical uncertainty (MSWD = 5.3, p = 0.000).

Thirty Hf spots were analysed on 30 magmatic zircons (Figure 4e). Excluding two outliers, one of which is also an outlier in O isotope analysis, the remaining 28 analyses range from εHf_t = 0.282254 to 0.282393, with an arithmetic mean $^{176}Hf/^{177}Hf_{420.9\ Ma}$ of 0.282328 ± 0.000077 (2SD; $\varepsilon Hf_{420.9\ Ma}$ = −6.5 ± 2.7), a weighted mean $^{176}Hf/^{177}Hf_{420.9\ Ma}$ of 0.282328 ± 0.000015, and scatter beyond analytical uncertainty (MSWD = 2.8, p = 0.000).

Inboard Thomson Orogen samples

The samples in this group were emplaced at least 100 km from the LTBS in the Thomson Orogen (Figure 2). The Thomson Orogen is generally composed of covered Neoproterozoic to Ordovician metasedimentary and metavolcanic rocks (Purdy *et al*., 2016). Owing to sparse outcrop and thick cover by sediments and sedimentary rocks in this region, samples of igneous rock are not common. Granite exposures outcrop along the Eulo Ridge, a series of basement inliers with sparse surface expression (Bultitude & Cross, 2013). Elsewhere, basement drill core provides the only means of sampling *in situ* igneous material.

The scarcity of samples meant that we did not have any available samples from our chosen time window, but other researchers have analysed samples relevant to this study. Cross *et al*. (2018) report U–Pb, O and Hf isotope data from the 425.4 ± 6.6 Ma S-type Ella Granite from the base of the ELLA 1 petroleum well drilled by Delhi in 1986 and the 419.1 ± 2.5 Ma S-type Hungerford Granite. In addition, the 401.8 ± 3.1 Ma I-type Tinchelooka Diorite (Bodorkos *et al*., 2013) was analysed to aid in coverage. This sample is slightly younger, and it is from a SW–NE-trending region of high magnetic intensity associated with the Culgoa Lineament (Doublier *et al*., 2018).

Tinchelooka Diorite

Bodorkos *et al*. (2013) documented SHRIMP U–Pb isotope analyses of this sample of the Tinchelooka Diorite (2002537). Twenty-eight analyses were performed on 20 zircons. Twenty of these analyses group to give a magmatic crystallisation age of 401.8 ± 3.1 Ma. Seven analyses between 2989 Ma and 424 Ma were interpreted as inherited, and one grain was interpreted to be affected by loss of radiogenic Pb.

Nineteen O isotope analyses were performed on 19 magmatic zircons (Figure 4f). Sixteen of the analyses range between $\delta^{18}O$ = 5.00 and 6.83‰, with a weighted mean of 6.25 ± 0.27‰ (95% CI), an arithmetic mean of 6.25 ± 0.92‰ (2SD) and scatter beyond analytical uncertainty (MSWD = 4.1, p = 0.000). Three analyses in a second group (as identified in the Hf results, Figure 4d) have $\delta^{18}O$ values of 6.75, 7.35 and 7.61.

Nineteen Hf isotope analyses were performed on 12 magmatic zircons (Figure 4f). Rejecting two spots owing to high analytical uncertainty, the remainder fall into two groups: the first group consists of 14 analyses that range from εHf_t = 0.282628 to 0.282712 and form a statistically coherent weighted mean $^{176}Hf/^{177}Hf_{401.8\ Ma}$ of 0.282661 ± 0.000016 (95% CI, $\varepsilon Hf_{401.8\ Ma}$ = +4.9 ± 0.5; MSWD = 1.2, p = 0.30). The second group (three analyses) range from εHf_t = 0.282465 to 0.282472 and give a weighted mean $^{176}Hf/^{177}Hf_{401.8\ Ma}$ of 0.282469 ± 0.000051 (95% CI, $\varepsilon Hf_{401.8\ Ma}$ = −1.9 ± 1.8; MSWD = 0.03, p = 0.97). The significance of this second group is unknown; it may represent a different but approximately coeval batch of magma that assimilated a greater amount of (meta)sedimentary material.

Discussion

Statistical treatment and depiction of data

When we apply statistical grouping to our data, we find that most of our samples have Hf isotopic results that form statistically coherent groupings with MSWDs that approach 1. This suggests that in many cases the Hf isotopic compositions of these rocks are homogeneous within the limits of analytical uncertainty, either because these granites originate from a single homogeneous source or because mixing of multiple sources was efficient enough to homogenise the Hf isotopic compositions, at least at sample-scale.

Oxygen-isotope values are more scattered, but it is unclear whether this is due to analytical, syn- or post-crystallisation effects. Oxygen is more susceptible to disturbance than U, Th, Pb or Hf in zircon (Cherniak & Watson, 2001; Cherniak *et al*., 1997; Watson & Cherniak, 1997) so samples with evidence for post-crystallisation disturbance of U–Pb systematics (i.e. Pb loss) are also more likely to have experienced disturbance of their $\delta^{18}O$ values. We reduce, but do not eliminate, the impact of post-crystallisation disturbance by analysing zircon spots that do not appear to be disturbed in U–Pb isotope systematics. For example, the high number of U–Pb spots attributed to Pb loss in samples indicates a higher probability of oxygen isotope disturbance across all zircons from the sample.

Where data scatter beyond the limits of analytical uncertainty, it is less statistically valid to apply a weighted mean calculation to a population that may have two or more distinguishable components. However, in the interests of applying a consistent statistical treatment to all data, and also to enable the use of MSWD to assess statistical coherence and test for the presence or absence of such complexity, we report both weighted and arithmetic means in Table 1.

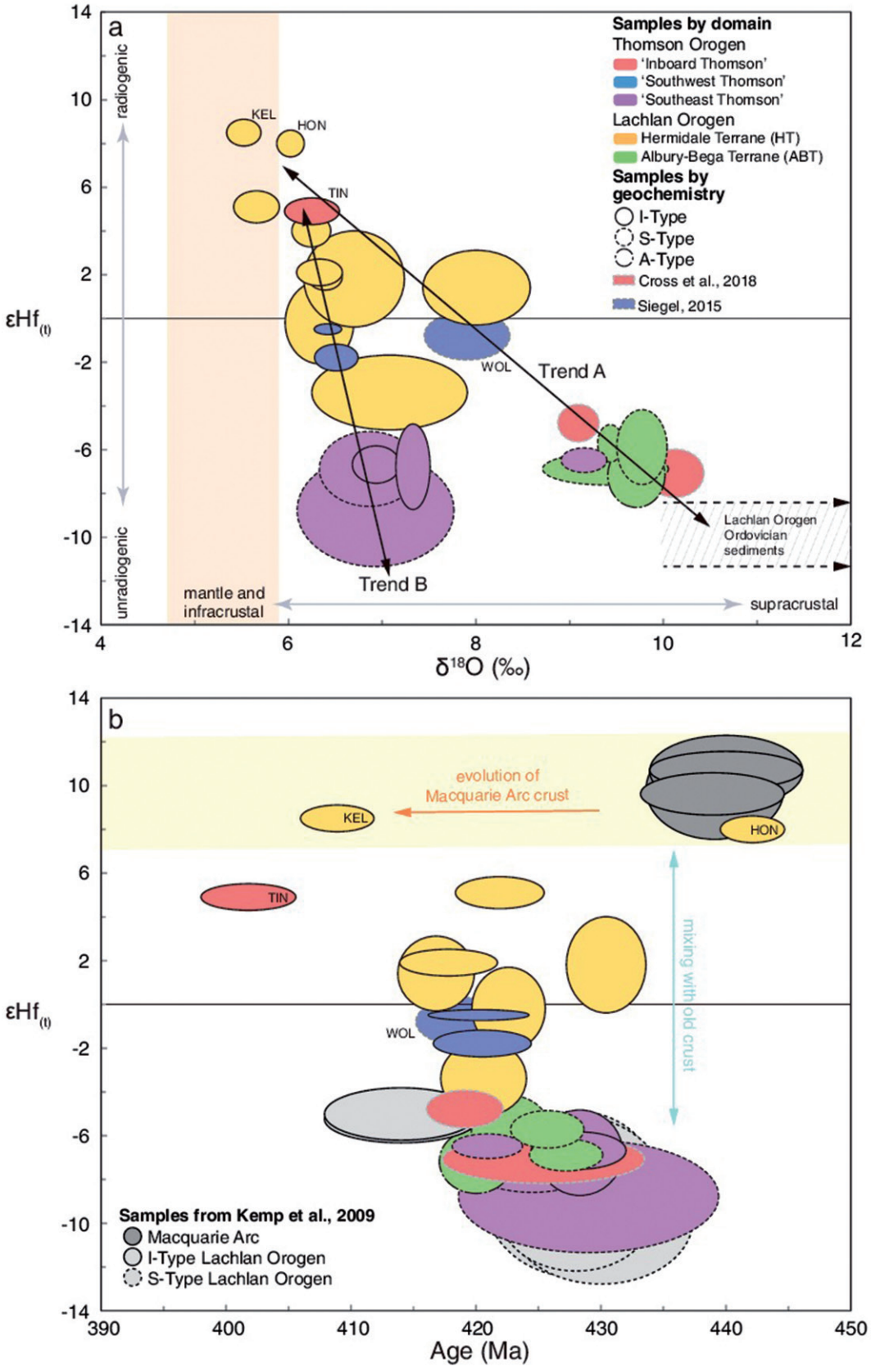

Figure 5. (a) εHf_t vs $\delta^{18}O$, and (b) εHf_t vs age. Ellipses represent the samples in this study, coloured by region as outlined in the text and shown in Figure 2. Labelled ellipses: HON, Honeybugle Complex diorite; KEL, Mount Kelly Granite; TIN, Tinchelooka Diorite; WOL, Wolgolla Granite. The outlines of the ellipses represent the geochemical grouping of each sample. The horizontal black line represents CHUR at $\varepsilon Hf_t = 0$. In the upper plot, the mantle-like window (5.3 ± 0.6‰, 2SD; Valley, 2005) is shown as an orange band. The lower plot includes data from Kemp *et al.* (2009), coloured grey. An evolution line of 'Macquarie Arc-like' crust is shown as a yellow band on the lower plot, with a $^{176}Lu/^{177}Hf$ composition of 0.023 (estimated from bulk-rock geochemical data in Kemp *et al.*, 2009). All plotted data are weighted mean ± 95% confidence interval, except for Kemp *et al.* (2009) data, which is plotted as arithmetic mean ± 2 standard deviations. Where the age uncertainty was not provided by Kemp *et al.* (2009), data points were assigned an arbitrary value of ± 5 Ma (95% CI).

Twenty-five samples are plotted in Figure 5 using weighted means ± 95% confidence intervals. The uncertainties plotted are smaller than ±2SD uncertainties, but the size of the error ellipses in Figure 5 reflects both scatter in the population and the number of analyses of the population. Larger error ellipses reflect more scattered data, fewer data points in the population or both, giving a visual indication of the reliability of the calculated weighted mean.

Isotopic trends

Ignoring the Triassic Midway granites in the Hermidale Terrane, the range of U–Pb ages of granites analysed for O and Lu–Hf isotopes in this study spans approximately 40 million years (440–400 Ma; Figure 5b). Despite this relatively narrow time window (which precludes significant secular variation in the isotopic nature of the source regions), Figure 5a illustrates the wide range of εHf_t and $\delta^{18}O$ values measured across the area of interest, a range that cannot be explained by simple two-component mixing between a single radiogenic source and a single unradiogenic source.

Rather, the data in Figure 5a appear to define two distinct mixing lines. Both have an endmember with radiogenic Hf and mantle-like $\delta^{18}O$ values; one has an unradiogenic-Hf endmember with elevated $\delta^{18}O$ values (Trend A), and the other has an unradiogenic-Hf endmember with more subdued $\delta^{18}O$ values (Trend B).

The unradiogenic endmember with elevated $\delta^{18}O$ values (Trend A) is most strongly represented in the Albury-Bega Terrane (Figure 5a). These rocks are unradiogenic (mean $\varepsilon Hf_t = -7.2$ to -5.7) and strongly supracrustral (mean $\delta^{18}O = 9.37$ to 9.78‰, Table 1). The Brewarrina Granite, in the southeast Thomson Orogen near the Mount Oxley Fault has a similar isotopic character ($\varepsilon Hf_t = -6.5$, $\delta^{18}O = 9.16$‰), as do the Ella Granite (1586685, 425.4 Ma, $\varepsilon Hf_t = -6.4$, $\delta^{18}O = 10.3$‰; Cross *et al*., 2018) and the Hungerford Granite (2122055, 419.1 Ma, $\varepsilon Hf_t = -4.6$, $\delta^{18}O = 9.3$‰; Cross *et al*., 2018), both from the interior of the southern Thomson Orogen (Figure 2).

Conversely, the unradiogenic endmember with less elevated $\delta^{18}O$ values (Trend B) is most strongly expressed in the Cuttaburra region. These drill-core samples are unradiogenic (mean $\varepsilon Hf_t = -8.8$ to -6.7) but less supracrustal (mean $\delta^{18}O = 6.86$ to 7.33‰) relative to the other unradiogenic endmember.

The common, radiogenic-Hf and mantle-like $\delta^{18}O$ value endmember is represented most strongly in granites from the Hermidale Terrane, and in the Tinchelooka Diorite. These granites are more radiogenic (εHf_t up to $+8.5$) and mantle-like/infracrustal ($\delta^{18}O$ as low as 5.52‰).

Other samples appear to be mixtures of two of these three components, but only between radiogenic–unradiogenic εHf pairs, and not between the two unradiogenic endmembers. Given the complexity of granite formation, it is unlikely that any samples represent pure endmember compositions. The following sections discuss possible explanations for these isotopic patterns, with particular emphasis on spatial trends that can be related to previously proposed tectonostratigraphic subdivision of the Lachlan and Thomson orogens. These major spatial trends are illustrated in Figure 6.

High $\delta^{18}O$–unradiogenic εHf endmember of Trend A

Middle to upper Silurian S-type magmatic rocks of the northern Albury-Bega Terrane display unradiogenic εHf_t values and elevated $\delta^{18}O$ values. Our results are consistent with measured Hf isotope ratios from granites from further south in the Lachlan Orogen (Kemp, Hawkesworth, Collins, Gray, & Blevin, 2009; Figure 5b). The limited range of εHf_t and $\delta^{18}O$ mean values (relative to the entire range across the 22 samples reported here) identified across much of the Lachlan Orogen indicates remarkable uniformity in the source region over a large spatial extent (hundreds of kilometres).

The source of S-type Lachlan Orogen granites has long been attributed to a metasedimentary origin (e.g. Chappell & White, 1992), commonly attributed to the Ordovician turbiditic metasediments that exist across much of the Lachlan Orogen (e.g. McCulloch & Chappell, 1982). The bulk-rock εNd signature of Ordovician Lachlan Orogen metasediments has been measured by McCulloch and Chappell (1982; State Circle Shale $\varepsilon Nd = -9.7$; Cooma Gneiss $\varepsilon Nd = -8.3$) and McCulloch and Woodhead (1993; country rock surrounding the Bega Batholith, $\varepsilon Nd = -10.5, -9.9, -9.7, -9.5$). We use the terrestrial trend of Vervoort, Patchett, Blichert-Toft, and Albarède (1999; $\varepsilon Hf = 1.36\varepsilon Nd + 2.95$) to convert these values to estimates of εHf (we assume no isotopic decoupling), giving an estimate of $\varepsilon Hf = -11.3$ to -8.3 for bulk Lachlan Orogen Ordovician metasediments. This range is plotted on Figure 5a, with $\delta^{18}O > 10$‰ as per the Eiler (2001) range for clastic sediments. The Albury-Bega Terrane samples from this study plot in more radiogenic and lower $\delta^{18}O$ space, suggesting that even the most supracrustal and unradiogenic granites in this study are not formed purely from melting of this supracrustal source, and do not represent true endmember composition.

Furthermore, upper Silurian S-type granites with very similar εHf_t and $\delta^{18}O$ values appear to be widespread on the northern side of the LTBS, across the breadth of the southern Thomson Orogen from Ella Granite in southwestern Queensland, through the Hungerford Granite in the interior, to the Brewarrina Granite in the east, proximal to the Macquarie Arc. This suggests that supracrustal rocks of broadly similar isotopic character floor much of both the Albury-Bega Terrane and the southern Thomson Orogen. This may indicate some geological continuity of the Lachlan Orogen into the Thomson Orogen. Alternatively, there may be another isotopically similar supracrustal source in the Thomson Orogen with no genetic relationship to the source in the Lachlan Orogen.

Low $\delta^{18}O$–unradiogenic εHf endmember of Trend B

On the northern side of the central (east–west-trending) region of the LTBS, mid-Silurian granites in the Cuttaburra region display unradiogenic εHf_t values spanning a range similar to that observed in the Albury-Bega Terrane ($\varepsilon Hf_t =$

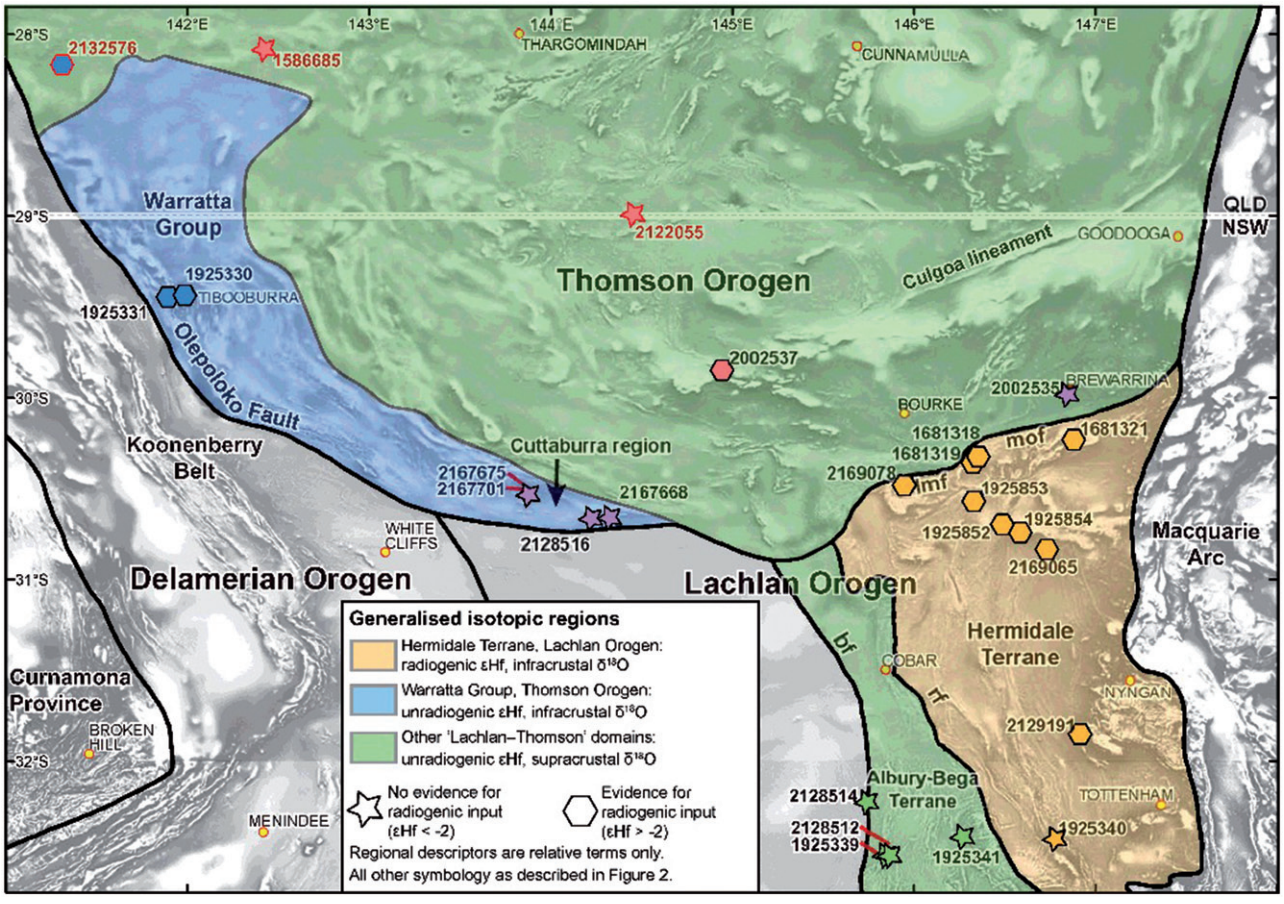

Figure 6. Map summarising generalised regions of Lu–Hf and O-isotopic similarity based on the data from this study. Samples are coloured by domain: red, 'Inboard Thomson'; blue, 'Southwest Thomson'; purple, 'Southeast Thomson'; orange, Hermidale Terrane; green, Albury-Bega Terrane. Symbols show whether there is evidence for radiogenic input: hexagon, $\varepsilon Hf > -2$; star, $\varepsilon Hf < -2$. Samples outlined in red and with red sample numbers are from other publications—refer to text. Major crustal boundaries and faults are marked with black lines, following those illustrated in Glen *et al.* (2009, 2013) and Korsch and Doublier (2015). The Lachlan–Thomson Boundary Structures (LTBS) consist of the Olepoloko Fault; lmf, Little Mountain Fault; and mof, Mount Oxley Fault; bf, Boothergandra Fault; rf, Rookery Fault System. The extent of the Warratta Group (blue) is based on interpretation by Purdy *et al.* (2018). Towns are marked by small yellow spots, and the QLD–NSW border is marked by a dashed line.

–8.8 to –6.7). They are, however, distinct in terms of their $\delta^{18}O$ values, which are only slightly elevated above the mantle-like window ($\delta^{18}O = 6.9$–7.3‰). The Cuttaburra granites are interpreted to intrude the upper Cambrian to Lower Ordovician Warratta Group (Greenfield *et al.*, 2010), a unit with little surface expression but significant sub-surface extent (Purdy *et al.*, 2018).

Similarly subdued $\delta^{18}O$ values were measured in the upper Silurian I-type rocks of the Tibooburra Suite (*ca* 420 Ma, $\varepsilon Hf_t = -1.8$ to -0.5, $\delta^{18}O = 6.4$ to 6.5‰) in the southwestern Thomson Orogen where they intrude outcropping rocks of the Warratta Group (Figure 6). These Tibooburra rocks have a stronger isotopic influence from a radiogenic component (Figure 5a). The combined Cuttaburra and Tibooburra data indicate that granites intruding the domain interpreted as Warratta Group (Figure 6) have an isotopically distinct source component different to the supracrustal source component flooring much of the northern Albury-Bega Terrane and southern Thomson Orogen. The muted $\delta^{18}O$ values of the region suggests that this source component may be infracrustal rather than supracrustal, for example a meta-igneous source.

Low $\delta^{18}O$–radiogenic εHf endmembers of Trend A and B

Across much of the study region, granites seem to have formed from the isotopic combination of the unradiogenic sources outlined above with one or more radiogenic sources with mantle-like/infracrustal isotopic character. The potential identity of this component varies with region, and so we will discuss options region-by-region, for (1) the Hermidale Terrane, (2) the southwest Thomson Orogen and (3) the inboard southern Thomson Orogen.

Hermidale Terrane

In the northeastern Lachlan Orogen, the Hermidale Terrane represents a crustal segment isotopically distinct from both the Albury-Bega Terrane to the west, and the Thomson Orogen to the north. In general, the samples analysed are Lower Devonian I-type granites (although the Honeybugle Complex is lower Silurian and the Midway granites are Triassic), their εHf_t values are significantly more radiogenic ($\varepsilon Hf_t = -3.4$ to $+8.5$) than elsewhere, and $\delta^{18}O$ values ($\delta^{18}O = 5.5$ to 8.0‰) are much more mantle-like/infracrustal.

These measured Hf–O values are broadly consistent with two-component mixing between a radiogenic-εHf_t, mantle-like-$\delta^{18}O$ source and an unradiogenic-εHf_t, elevated-$\delta^{18}O$ values supracrustal source (Trend A; Figure 5a).

Ordovician arc rocks, possibly related to the Macquarie Arc, are one potential identity of the radiogenic source component. The Macquarie Arc outcrops to the east of the Hermidale Terrane and to the east of the Albury-Bega Terrane further south of this study area. Seismic-reflection profiling in the Temora region provides evidence that Ordovician volcanic rocks underlie the eastern part of the Wagga Belt in the Albury-Bega Terrane, representing a westerly continuation of Macquarie Arc rocks undercover (Glen *et al*., 2002). Although this is not direct evidence that the same geometry exists under the Hermidale Terrane, the seismic-reflection profiling evidence does permit Ordovician arc rocks to extend west of the outcropping Macquarie Arc and underlie the Hermidale Terrane.

Kemp *et al*. (2009) analysed Hf isotopes on zircons from Macquarie Arc rocks, and they are plotted relative to our samples in Figure 5b. The Honeybugle Complex (2129191) is the most radiogenic sample in this study, and overlaps the Macquarie Arc field in both age and Hf isotopic composition. The isotopic similarity between these rocks, and their close spatial proximity, suggests that the Honeybugle Complex may be closely genetically related to the Macquarie Arc. The Mount Kelly Granite (1681321) is younger than the youngest known Macquarie Arc rocks, but falls within the Hf evolution window for the Macquarie Arc, consistent with being sourced from Macquarie Arc-like material at depth, with little mixing with other sources. All other samples in the Hermidale Terrane fall between the supracrustal source component composition and the Macquarie Arc evolution window (Figure 5b), and all isotopic variations in this region can be explained by variable mixing between the two components.

There is a loose correlation between radiogenic Hf signature and proximity to the Macquarie Arc, which may suggest thickening of this component towards the surface expression of the arc, but may also be explained by a range of other geological processes not easily evaluated here, such as depth of melting.

Others (Keay *et al*., 1997; Kemp *et al*., 2005b) have considered Ordovician arc rocks as an end member source component for granites in other locations in the Lachlan Orogen, however these researchers favoured direct mantle input at the time of granite generation rather than remelting of emplaced arc rocks. Our isotopic study cannot resolve between the two possibilities (or whether the composition may result from a combination of both options), partly because all rocks in this study incorporate some degree of supracrustal influence, and partly owing to the isotopic similarity of the potential radiogenic sources.

The younger Midway granites have mantle-like O and Hf isotope signatures that can be derived from the same Trend A mixed source as the older granites in the region. Additional Triassic mantle input is not required to explain the O–Hf isotopic signature of these granites, but, as with the other samples, we cannot exclude this possibility.

Southwest Thomson Orogen

Farther to the west and within the interpreted extent of the Warratta Group (Figure 6), the Tibooburra samples have an Hf isotope signature that is also suggestive of contribution from a radiogenic source component. One viable source is the Mount Wright Arc, which occurs nearby to the southwest. The radiogenic component expressed in the Tibooburra granites may reflect Mount Wright Arc-type material at depth in this region, beneath the Warratta Group. This would be consistent with a northeasterly dip for the Olepoloko Fault in this region, juxtaposing Warratta Group in the hanging wall with Mount Wright Arc rocks in the footwall.

The geometry of the Mount Wright Arc proposed by Greenfield *et al*. (2011) is consistent with radiogenic material occurring along the Tibooburra region and possibly north (i.e. inclusive of the Wolgolla Granite for which εHf and $\delta^{18}O$ also indicate a radiogenic source component), but not in the Cuttaburra region.

Keay *et al*. (1997) proposed a three-component model for granite genesis in the Lachlan Orogen. Their components were an Ordovician turbidite component, a depleted mantle component and a mafic crustal component. Their mafic crustal component was attributed to Cambrian greenstones, the εNd signature of which (Nelson, Crawford, & McCulloch, 1984) spans the equivalent of our entire εHf range for Trend B (Figure 5a). Given geochemical indications that the Cambrian greenstones, preserved in the Lachlan Orogen in Victoria, are likely to have assimilated variable amounts of sedimentary material during formation (Whelan, Hergt, & Woodhead, 2007), it is unsurprising that the greenstones span a wide range of εNd (and presumably εHf).

Trend B (Figure 5a) is consistent with Keay's model, where radiogenic mafic greenstone-type rocks are emplaced in the crust and are represented by the radiogenic endmember of Trend B. These mafic rocks may have assimilated variable amounts of sedimentary material, so emplaced mafic rocks could be more unradiogenic than the pure mantle-derived melt. Subsequent melting of these greenstone belts during granite generation is also likely to melt spatially associated sedimentary units, which will also drive the isotopic signature to a more unradiogenic isotopic character. One potential issue with this model comes from the more muted $\delta^{18}O$ values than might be expected if the unradiogenic component was contaminated by sediment.

If greenstone rocks were the source of granites in the southwest Thomson Orogen, this would suggest that there may be some genetic relationship between the Mount Wright Arc and the greenstone belts in Victoria. If correct, this in turn demonstrates another commonality between the Lachlan Orogen and the southern Thomson Orogen.

Analysis of geochemical data led to the interpretation by Greenfield *et al*. (2010) that the Tibooburra Suite granites formed by partial melting of a mantle source that was

contaminated by crustal sources. A direct mantle source is also consistent with our isotopic data.

Tinchelooka Diorite

The marginally younger (*ca* 402 Ma) I-type Tinchelooka Diorite is spatially associated with the highly magnetic Culgoa lineament in the central southern Thomson Orogen, and is characterised by significantly more radiogenic (albeit bimodal) εHf_t and $\delta^{18}O$ values elevated only marginally above the 'mantle-like' window. The geology of this region is poorly known, so the identity of the radiogenic source component of the Tinchelooka Diorite is much more cryptic.

Mafic/ultramafic samples are identified along the Culgoa lineament (Doublier *et al*., 2018). The age of these mafic/ultramafic Culgoa lineament rocks (at depth) is unknown, but if they were the right age (i.e. slightly but not significantly older than the diorite) they might have influenced the isotopic signature of the Tinchelooka Diorite. Alternatively, the radiogenic source for the Tinchelooka Diorite may be caused by direct mantle input.

Nature of the LTBS—testing regional models

The nature of the LTBS appears to change in character across the southern margin of the Thomson Orogen. To the west, previous authors have outlined the evidence for the boundary between the Delamerian Orogen and the Thomson Orogen occurring at or near the Olepoloko Fault in the southwest of the Thomson Orogen (e.g. Glen *et al*., 2013; Greenfield *et al*., 2010). The isotopic results for the Tibooburra Suite provide evidence that the Thomson Orogen and Delamerian Orogen must have been in their current configuration by 420 Ma, if these granites record the influence of arc material in their source regions. This in turn suggests that subsequent late Paleozoic SSE-directed movement on the eastern segment of the Olepoloko Fault (which folded *ca* 385 Ma Tabberabberan structures in the Cobar Basin into E–W orientations; Downes *et al*., 2016) did not generate significant strike-slip movement on the western segment of the Olepoloko Fault (which separates the Delamerian Orogen from the southwest Thomson Orogen).

Our results also show an isotopic distinction between the southeastern Thomson Orogen and the Hermidale Terrane (Figure 6). The Hermidale Terrane has a distinct mixture of radiogenic and unradiogenic source components that appears to terminate at major fault boundaries. The Little Mountain–Mount Oxley Fault and the Rookery Fault appear to define the limits of underlying radiogenic material (potentially Macquarie Arc-related).

There is no distinguishable Hf or O isotopic difference between the bulk of the southern Thomson Orogen and the bulk of the Lachlan Orogen, as represented by the Albury-Bega Terrane. In the south–central region of this study area, these two regions adjoin each other, and orogen-bounding faults have not been identified in this area. The faulting to the west (Olepoloko Fault) and the faulting to the east (Little Mountain Fault and Mount Oxley Fault) are possibly unrelated structures separated by a narrow region that remains an unbroken connection between the stratigraphically coherent Lachlan Orogen and southern Thomson Orogen.

There is no unique solution that resolves the available isotopic evidence; however, some inferences can be drawn. Although data coverage remains sparse, there is a lack of radiogenic Hf and mantle-like $\delta^{18}O$ values along the southern margin of the Thomson Orogen that would support the presence of an intact east–west-trending volcanic arc related to north-dipping subduction along the Olepoloko Fault as inferred by Glen (2013) and Gray and Foster (2004).

Evidence that the Little Mountain–Mount Oxley Fault system to the east represents the boundary between the Thomson Orogen and the Lachlan Orogen may be confounded by the presence of the Hermidale Terrane, an isotopically unique section of crust more strongly influenced by a radiogenic source component than the surrounding regions to the north, west or south.

The relationship between the Thomson Orogen and the Lachlan Orogen could be further tested by finding distinctions between sections of crust, which are truly representative of the bulk of these orogens, namely the bulk of the southern Thomson Orogen excluding the far-western component and the magnetic high associated with the Culgoa lineament, and the Lachlan Orogen as represented by the Albury-Bega Terrane. Despite the limited data coverage caused by sparse sample availability, it is clear that the Thomson Orogen is more internally complex than current mapping reveals.

Conclusions

The isotopic character of all samples in this study can be best described by three-component mixing of variable amounts of high $\delta^{18}O$–unradiogenic εHf source component (across Lachlan Orogen and most of the Thomson Orogen; Trend A), a high $\delta^{18}O$–unradiogenic εHf source component (confined to the Warrata Group in the Thomson Orogen; Trend B) and one or more low $\delta^{18}O$–radiogenic εHf source components (arc-related, or direct mantle input; Trend A and B).

Data coverage remains sparse owing to the paucity of appropriate available samples, especially within the Thomson Orogen; however, we have not yet identified any contrast in Lu–Hf or O-isotopic character between the northern Lachlan Orogen Albury-Bega Terrane and the southern Thomson Orogen.

We detect potential arc influences from the Macquarie Arc in intrusions in the Hermidale Terrane into the northwest Lachlan Orogen, and from the Mount Wright Arc in intrusions into the Warratta Group in the southwest Thomson Orogen; however, our isotopic data cannot distinguish between these sources and granite formation as a result of direct mantle input into the granite source region.

The status of the southern Thomson boundary structure is not yet clear; however, our results demonstrate that isotopic variations within both the Thomson Orogen and the Lachlan

Orogen appear to be larger than any north-to-south variation across the central section of the LTBS.

This study has highlighted that the Hf and O isotopic character of the bulk of the northern Lachlan Orogen and the bulk of the southern Thomson Orogen are indistinguishable, and has also highlighted regions of different isotopic character, specifically in the Hermidale Terrane, and the crust underlying the Warratta Group.

Acknowledgements

We thank our collaborative partner, the Geological Survey of New South Wales (GSNSW) for their mapping and sampling efforts and for permission to use SHRIMP mounts for isotopic studies. We thank Phil Blevin (GSNSW) for giving permission to use some analyses that were paid for by the Geological Survey of New South Wales. This project would not have been possible without the foresight and diligence of Lance Black, Chris Foudoulis and David DiBugnara for creating high-quality SHRIMP mounts, and for systematic archival of mounts, mount maps and zircon photographs. We thank the attendees of the southern Thomson Orogen workshops for their encouragements and insights, and Geoff Fraser for his significant feedback and discussions during the early phases of this paper. Thank you to the GA internal reviewers Geoff Fraser and Natalie Kositcin. We thank Bill Collins and an anonymous reviewer for comments that greatly improved this paper. This paper is published with the permission of the CEO of Geoscience Australia.

Disclosure statement

No potential conflict of interest was reported by the authors.

Supplementary papers

Appendix A. Sample selection and preparation, analytical methods and data processing.
Table A1. Lu–Hf session information (Excel file).
Table A2. Oxygen isotope session information (Excel file).
Table A3. Lu–Hf reference results (Excel file).
Table A4. Oxygen isotope reference results (Excel file).
Table A5. Lu–Hf and oxygen isotope sample results (Excel file).

ORCID

K. Waltenberg http://orcid.org/0000-0002-1629-0597
S. Bodorkos http://orcid.org/0000-0001-8605-0276
R. Armstrong http://orcid.org/0000-0002-3062-0679

References

Armistead, S. E., & Fraser, G. L. (2015). *New SHRIMP U–Pb zircon ages from the Cuttaburra and F1 prospects, southern Thomson Orogen, New South Wales*. Canberra, ACT: Geoscience Australia Record 2015/20. doi:10.11636/Record.2015.020

Armistead, S. E., Skirrow, R. G., Fraser, G. L., Huston, D. L., Champion, D. C., & Norman, M. D. (2017). *Gold and intrusion-related Mo–W mineral systems in the southern Thomson Orogen, New South Wales*. Canberra, ACT: Geoscience Australia Record 2017/05. doi:10.11636/Record.2017.005

Baertschi, P. (1976). Absolute ^{18}O content of standard mean ocean water. *Earth and Planetary Science Letters*, *31*(3), 341–344. doi:10.1016/0012-821X(76)90115-1

Bennett, V. C., & DePaolo, D. J. (1987). Proterozoic crustal history of the western United States as determined by neodymium isotopic mapping. *Geological Society of America Bulletin*, *99*(5), 674–685. doi:10.1130/0016-7606(1987)99<674:pchotw>2.0.co;2

Black, L. P. (2006). *SHRIMP U–Pb zircon ages obtained during 2005/2006 for NSW Geological Survey projects*. Maitland, NSW: Geological Survey of New South Wales Report GS2006/821. Retrieved from http://search.geoscience.nsw.gov.au/report/R00041608

Black, L. P. (2007). *SHRIMP U–Pb zircon ages obtained during 2006/07 for NSW Geological Survey projects*. Maitland, NSW: Geological Survey of New South Wales Report GS2007/298. Retrieved from http://search.geoscience.nsw.gov.au/report/R00041609

Blevin, P. L. (2011). *Petrological, chemical and metallogenic notes on the granites of the Bourke 250k sheet, NSW*. (PetroChem Consultants Pty Ltd Report D006218260). Retrieved from http://search.geoscience.nsw.gov.au/report/R00079974

Blevin, P. L., & Jones, M. (2004). Chemistry, age and metallogeny of the granites and related rocks of the Nymagee region, NSW. In K. G. McQueen & K. M. Scott (Eds.), *Proceedings of the Exploration Field Workshop Cobar Region* (pp. 15–19). Perth: CRC LEME Publication.

Blichert-Toft, J., & Albarède, F. (1997). The Lu–Hf isotope geochemistry of chondrites and the evolution of the mantle–crust system. *Earth and Planetary Science Letters*, *148*(1–2), 243–258. doi:10.1016/S0012-821X(97)00040-X

Bodorkos, S., Blevin, P. L., Eastlake, M. A., Downes, P. M., Campbell, L. M., Gilmore, P. J., … Trigg, S. J. (2015). *New SHRIMP U–Pb zircon ages from the central and eastern Lachlan Orogen, New South Wales; July 2013–June 2014*. Canberra, ACT: Geoscience Australia Record 2015/02. doi:10.11636/Record.2015.002

Bodorkos, S., Blevin, P. L., Simpson, C. J., Gilmore, P. J., Glen, R. A., Greenfield, J. E., … Quinn, C. D. (2013). *New SHRIMP U–Pb zircon ages from the Lachlan, Thomson and Delamerian Orogens, New South Wales: July 2009–June 2010*. Canberra, ACT: Geoscience Australia Record 2013/29. doi:10.11636/Record.2013.029

Brown, D. D., Carr, P. A., & Purdy, D. J. (2012). *Database of basement drill holes in the Thomson Orogen and Roma Shelf regions, Queensland*. Brisbane, Qld: Queensland Geological Record 2012/06.

Bultitude, R. J., & Cross, A. J. (2013). Granites of the Eulo Ridge. In P. A. Jell (Ed.), *Geology of Queensland* (pp. 166–167). Brisbane, QLD: Queensland Geological Survey Record 2015/02.

Burton, G. R. (2010). New structural model to explain geophysical features in northwestern New South Wales: Implications for the tectonic framework of the Tasmanides. *Australian Journal of Earth Sciences*, *57*(1), 23–49. doi:10.1080/08120090903416195

Burton, G. R., Trigg, S. J., & Black, L. P. (2007). A Middle Triassic age for felsic intrusions and associated mineralisation in the Doradilla prospect area, New South Wales. *Geological Survey of New South Wales Quarterly Notes*, *125*, 1–11. Retrieved from http://search.geoscience.nsw.gov.au/report/R00041872

Burtt, A. C., & Lockheed, A. E. (2008). *Annual Technical Report, EL 6850 Tringadee New South Wales for year ending 2nd August, 2008*. Maitland, NSW: Geological Survey of New South Wales Report GS2009/0265. Retrieved from http://search.geoscience.nsw.gov.au/report/R00079788

Carr, P. A., Purdy, D. J., & Brown, D. D. (2014). *Peeking under the covers; undercover geology of the Thomson Orogen*. Paper presented at the Australian Earth Sciences Convention, Newcastle, Australia.

Cawood, P. A., & Buchan, C. (2007). Linking accretionary orogenesis with supercontinent assembly. *Earth-Science Reviews*, *82*(3), 217–256. doi:10.1016/j.earscirev.2007.03.003

Champion, D. C. (2013). *Neodymium depleted mantle model age map of Australia: Explanatory notes and user guide*. Canberra, ACT: Geoscience Australia Record 2013/44. doi:10.11636/Record.2013.044

Champion, D. C. (2016). *Geodynamic synthesis of the Phanerozoic of eastern Australia*. Canberra, ACT: Geoscience Australia Record 2016/07. doi:10.11636/Record.2016.007

Chappell, B. W. (1979). Granites as images of their source rocks. *Geological Society of America Abstracts with Programs*, *11*(7), 400.

Chappell, B. W., & Stephens, W. E. (1988). Origin of infracrustal (I-type) granite magmas. *Earth and Environmental Science Transactions of the Royal Society of Edinburgh*, *79*(2–3), 71–86. doi:10.1017/s0263593300014139

Chappell, B. W., & White, A. J. R. (1992). I- and S-type granites in the Lachlan Fold Belt. In P. E. Brown & B. W. Chappell (Eds.), *The Second Hutton Symposium on the Origin of Granites and Related Rocks*. (pp. 1–26). Edinburgh: Transactions of the Royal Society of Edinburgh No. 83.

Cherniak, D. J., & Watson, E. B. (2001). Pb diffusion in zircon. *Chemical Geology*, *172*(1), 5–24. doi:10.1016/S0009-2541(00)00233-3

Cherniak, D. J., Hanchar, J. M., & Watson, E. B. (1997). Diffusion of tetravalent cations in zircon. *Contributions to Mineralogy and Petrology*, *127*(4), 383–390. doi:10.1007/s004100050287

Chisholm, E. I., Blevin, P. L., Downes, P. J., & Simpson, C. J. (2014). *New SHRIMP U–Pb zircon ages from the central Lachlan Orogen and Thomson Orogen, New South Wales*. Canberra, ACT: Geoscience Australia Record 2014/32. doi:10.11636/Record.2014.032

Collins, W. J. (2002). Nature of extensional accretionary orogens. *Tectonics*, *21*(4). doi:10.1029/2000tc001272

Crawford, A. J., & Keays, R. R. (1978). Cambrian greenstone belts in Victoria: Marginal sea–crust slices in the Lachlan Fold Belt of southeastern Australia. *Earth and Planetary Science Letters*, *41*(2), 197–208. doi:10.1016/0012-821X(78)90010-9

Cross, A. J., Purdy, D. J., Champion, D. C., Brown, D. D., Siégel, C., & Armstrong, R. A. (2018). Insights into the evolution of the Thomson Orogen from geochronology, geochemistry and zircon isotopic studies of magmatic rocks. *Australian Journal of Earth Sciences*, *65*, 987–1008. doi:10.1080/08120099.2018.1515791.

Doublier, M. P., Purdy, D. J., Hegarty, R. A., Nicoll, M. G., & Zwingmann, H. (2018). Structural elements of the southern Thomson Orogen (Australian Tasmanides): a tale of megafolds. *Australian Journal of Earth Sciences*, *65*, 943–965. doi:10.1080/08120099.2018.1526213.

Downes, P. M., Blevin, P. L., Armstrong, R., Simpson, C. J., Sherwin, L., Tilley, D. B., & Burton, G. R. (2016). Outcomes of the Nymagee mineral system study — an improved understanding of the timing of events and prospectivity of the central Lachlan Orogen. *Geological Survey of New South Wales Quarterly Notes*, *147*, 38 pp. Retrieved from http://search.geoscience.nsw.gov.au/report/R00076225

Eggins, S. M., Grün, R., McCulloch, M. T., Pike, A. W. G., Chappell, J., Kinsley, L., … Taylor, L. (2005). In situ U-series dating by laser-ablation multi-collector ICPMS: New prospects for Quaternary geochronology. *Quaternary Science Reviews*, *24*(23–24), 2523–2538. doi:10.1016/j.quascirev.2005.07.006

Eiler, J. M. (2001). Oxygen isotope variations of basaltic lavas and upper mantle rocks. *Reviews in Mineralogy and Geochemistry*, *43*(1), 319–364.

Fergusson, C. L., & Henderson, R. A. (2013). Thomson Orogen. In P. A. Jell (Ed.), *Geology of Queensland* (pp. 113–224). Brisbane, QLD: Geological Survey of Queensland.

Fraser, G. L., Gilmore, P. J., Fitzherbert, J. A., Trigg, S. J., Campbell, L. M., Deyssing, L., … Simpson, C. J. (2014). *New SHRIMP U–Pb zircon ages from the Lachlan, southern Thomson and New England orogens, New South Wales: February 2011–June 2013*. Canberra, ACT: Geoscience Australia Record 2014/53. doi:10.11636/Record.2014.053

Fraser, G. L., Kositcin, N., & Thorne, J. P. (in prep.). *New SHRIMP U–Pb zircon ages from the northern Lachlan Orogen, Thomson Orogen and Koonenberry Belt, New South Wales: April 2014–July 2015* (Unpublished Record). Canberra, ACT: Geoscience Australia.

Gardiner, N. J., Hickman, A. H., Kirkland, C. L., Lu, Y., Johnson, T., & Zhao, J.-X. (2017). Processes of crust formation in the early Earth imaged through Hf isotopes from the East Pilbara Terrane. *Precambrian Research*, *297*, 56–76. doi:10.1016/j.precamres.2017.05.004

Gatehouse, C. G. (1986). The geology of the Warburton Basin in South Australia. *Australian Journal of Earth Sciences*, *33*(2), 161–180. doi:10.1080/08120098608729357

Glen, R. A. (2005). The Tasmanides of eastern Australia. In A. P. M. Vaughan, P. T. Leat, & R. J. Pankhurst (Eds.), *Terrane Processes at the Margins of Gondwana* (pp. 23–96). London, UK: Geological Society Special Publication 246.

Glen, R. A. (2013). Refining accretionary orogen models for the Tasmanides of eastern Australia. *Australian Journal of Earth Sciences*, *60*(3), 315–370. doi:10.1080/08120099.2013.772537

Glen, R. A., Korsch, R. J., Direen, N. G., Jones, L. E. A., Johnstone, D. W., Lawrie, K. C., … Shaw, R. D. (2002). Crustal structure of the Ordovician Macquarie Arc, Eastern Lachlan Orogen, based on seismic-reflection profiling. *Australian Journal of Earth Sciences*, *49*(2), 323–348. doi:10.1046/j.1440-0952.2002.00925.x

Glen, R. A., Korsch, R. J., Hegarty, R., Saeed, A., Djomani, Y. P., Costelloe, R. D., & Belousova, E. (2013). Geodynamic significance of the boundary between the Thomson Orogen and the Lachlan Orogen, northwestern New South Wales and implications for Tasmanide tectonics. *Australian Journal of Earth Sciences*, *60*(3), 371–412. doi:10.1080/08120099.2013.782899

Glen, R. A., Percival, I. G., & Quinn, C. D. (2009). Ordovician continental margin terranes in the Lachlan Orogen, Australia: Implications for tectonics in an accretionary orogen along the east Gondwana margin. *Tectonics*, *28*(6), 1–17. doi:10.1029/2009tc002446

Gray, C. M. (1984). An isotopic mixing model for the origin of granitic rocks in southeastern Australia. *Earth and Planetary Science Letters*, *70*(1), 47–60. doi:10.1016/0012-821X(84)90208-5

Gray, D. R., & Foster, D. A. (2004). Tectonic evolution of the Lachlan Orogen, southeast Australia: Historical review, data synthesis and modern perspectives. *Australian Journal of Earth Sciences*, *51*(6), 773–817. doi:10.1111/j.1400-0952.2004.01092.x

Greenfield, J. E., Gilmore, P. J., & Mills, K. J. (Eds.). (2010). *Explanatory notes for the Koonenberry Belt geological maps*. Maitland, NSW: Geological Survey of New South Wales Bulletin 35.

Greenfield, J. E., Musgrave, R. J., Bruce, M. C., Gilmore, P. J., & Mills, K. J. (2011). The Mount Wright Arc: A Cambrian subduction system developed on the continental margin of East Gondwana, Koonenberry Belt, eastern Australia. *Gondwana Research*, *19*(3), 650–669. doi:10.1016/j.gr.2010.11.017

Hegarty, R., & Doublier, M. (2015). *Defining major structures and their depth extent under cover in the southern Thomson Orogen, New South Wales*. Paper presented at the 24th International Geophysical Conference and Exhibition, Perth, Western Australia.

Hellstrom, J., Paton, C., Woodhead, J., & Hergt, J. (2008). Software for spatially resolved LA-(QUAD and MC) ICPMS analysis. In P. Sylvester (Ed.), *Laser Ablation ICP–MS in the Earth Sciences: Current Practices and Outstanding Issues* (Vol. 40, pp. 343–348). Quebec: Mineralogical Association of Canada.

Ickert, R. B., Hiess, J., Williams, I. S., Holden, P., Ireland, T. R., Lanc, P., … Clement, S. W. (2008). Determining high precision, in situ, oxygen isotope ratios with a SHRIMP II: Analyses of MPI-DING silicate-glass reference materials and zircon from contrasting granites. *Chemical Geology*, *257*(1–2), 114–128. doi:10.1016/j.chemgeo.2008.08.024

Isaacs, D. (2000). *Evolution of the Nymagee region: Utilising geochemistry, geochronology and geophysics*. BSc (Honours) thesis, unpublished. Canberra, ACT: Australian National University.

Keay, S., Collins, W. J., & McCulloch, M. T. (1997). A three-component Sr–Nd isotopic mixing model for granitoid genesis, Lachlan Fold Belt, eastern Australia. *Geology*, *25*(4), 307–310. doi:10.1130/0091-7613(1997)025<0307:atcsni>2.3.co;2

Kemp, A. I. S., Hawkesworth, C. J., Collins, W. J., Gray, C. M., & Blevin, P. L. (2009). Isotopic evidence for rapid continental growth in an extensional accretionary orogen: The Tasmanides, eastern Australia. *Earth and Planetary Science Letters*, *284*(3–4), 455–466. doi:10.1016/j.epsl.2009.05.011

Kemp, A. I. S., Hawkesworth, C. J., Paterson, B. A., Foster, G. L., Kinny, P. D., Whitehouse, M. J., … EIMF. (2008). Exploring the plutonic–volcanic link: A zircon U–Pb, Lu–Hf and O isotope study of paired volcanic and granitic units from southeastern Australia. *Transactions of the Royal Society of Edinburgh–Earth Sciences*, *97*(4), 337–355. doi:10.1017/S0263593300001498

Kemp, A. I. S., Whitehouse, M. J., Hawkesworth, C. J., & Alarcon, M. K. (2005a). A zircon U–Pb study of metaluminous (I-type) granites of the Lachlan Fold Belt, southeastern Australia: Implications for the high/low temperature classification and magma differentiation processes. *Contributions to Mineralogy and Petrology*, *150*(2), 230–249. doi:10.1007/s00410-005-0019-6

Kemp, A. I. S., Wormald, R. J., Whitehouse, M. J., & Price, R. C. (2005b). Hf isotopes in zircon reveal contrasting sources and crystallization histories for alkaline to peralkaline granites of Temora, southeastern Australia. *Geology*, *33*(10), 797–800. doi:10.1130/g21706.1

Kirkegaard, A. G. (1974). Structural elements of the northern part of the Tasman Geosyncline. In A. K. Denmead, G. W. Tweedale, & A. F. Wilson (Eds.), *The Tasman Geosyncline – a symposium* (pp. 47–62). Brisbane, Queensland: Geological Society of Australia, Queensland Division.

Korsch, R. J., & Doublier, M. P. (2015). *Major crustal boundaries of Australia* [digital dataset]. Canberra, ACT: Geoscience Australia. doi:10.4225/25/555C181CC0EAE

McCulloch, M. T., & Chappell, B. W. (1982). Nd isotopic characteristics of S- and I-type granites. *Earth and Planetary Science Letters*, *58*(1), 51–64. doi:10.1016/0012-821X(82)90102-9

McCulloch, M. T., & Woodhead, J. D. (1993). Lead isotopic evidence for deep crustal-scale fluid transport during granite petrogenesis. *Geochimica et Cosmochimica Acta*, *57*, 659–674. doi:10.1016/0016-7037(93)90376-8

Mole, D. R., Fiorentini, M. L., Cassidy, K. F., Kirkland, C. L., Thebaud, N., McCuaig, T. C., … Miller, J. (2013). Crustal evolution, intra-cratonic architecture and the metallogeny of an Archaean craton. In G. R. T. Jenkin, P. A. J. Lusty, I. McDonald, M. P. Smith, A. J. Boyce, & J. J. Wilkinson (Eds.), *Ore deposits in an evolving earth* (pp. 23–80). Geological Society of London, Special Publication 393. doi:10.1144/SP393.8

Mole, D. R., Fiorentini, M. L., Thebaud, N., Cassidy, K. F., McCuaig, T. C., Kirkland, C. L., … Barnes, S. J. (2014). Archean komatiite volcanism controlled by the evolution of early continents. *Proceedings of the National Academy of Sciences*, *111*(28), 10083–10088. doi:10.1073/pnas.1400273111

Moresi, L., Betts, P. G., Miller, M. S., & Cayley, R. A. (2014). Dynamics of continental accretion. *Nature*, *508*(7495), 245–248. doi:10.1038/nature13033

Murray, C. G. (1994). *Basement cores from the Tasman Fold Belt System beneath the Great Artesian Basin in Queensland*. Brisbane, QLD: Geological Survey of Queensland Record 1994/10.

Murray, C. G., & Kirkegaard, A. G. (1978). The Thomson Orogen of the Tasman Orogenic Zone. *Tectonophysics*, *48*(3–4), 299–325. doi:10.1016/0040-1951(78)90122-1

Nelson, D. R., Crawford, A. J., & McCulloch, M. T. (1984). Nd–Sr isotopic and geochemical systematics in Cambrian boninites and tholeiites from Victoria, Australia. *Contributions to Mineralogy and Petrology*, *88*(1), 164–172. doi:10.1007/bf00371420

Norman, M. (2004). Zircon age dating of sample TYM-063, Fountaindale Granodiorite (Report A04-2004, unpublished). Canberra: Australian National University.

Paton, C., Hellstrom, J., Paul, B., Woodhead, J., & Hergt, J. (2011). Iolite: Freeware for the visualisation and processing of mass spectrometric data. *Journal of Analytical Atomic Spectrometry*, *26*(12), 2508–2518. doi:10.1039/C1JA10172B

Paton, C., Woodhead, J. D., Hellstrom, J. C., Hergt, J. M., Greig, A., & Maas, R. (2010). Improved laser ablation U–Pb zircon geochronology through robust downhole fractionation correction. *Geochemistry, Geophysics, Geosystems*, *11*(3), Q0AA06. doi:10.1029/2009gc002618

Percival, I. G., & Glen, R. A. (2007). Ordovician to earliest Silurian history of the Macquarie Arc, Lachlan Orogen, New South Wales. *Australian Journal of Earth Sciences*, *54*(2–3), 143–165. doi:10.1080/08120090601146789

Purdy, D. J., Cross, A. J., Brown, D. D., Carr, P. A., & Armstrong, R. A. (2016). New constraints on the origin and evolution of the Thomson Orogen and links with central Australia from isotopic studies of detrital zircons. *Gondwana Research*, *39*, 41–56. doi:10.1016/j.gr.2016.06.010

Purdy, D. J., Hegarty, R., & Doublier, M. P. (2018). Basement geology of the southern Thomson Fold Belt. *Australian Journal of Earth Sciences*, *65*, 893–916. doi:10.1080/08120099.2018.1453547

Quinn, C. D., Percival, I. G., Glen, R. A., & Xiao, W.-J. (2014). Ordovician marginal basin evolution near the palaeo-Pacific east Gondwana margin, Australia. *Journal of the Geological Society, London*, *171*(5), 723–736. doi:10.1144/jgs2012-034

Scheibner, E. (1973). A plate tectonic model of the Palaeozoic tectonic history of New South Wales. *Journal of the Geological Society of Australia*, *20*(4), 405–426. doi:10.1080/00167617308728826

Scherer, E., Münker, C., & Mezger, K. (2001). Calibration of the Lutetium–Hafnium clock. *Science*, *293*(5530), 683–687. doi:10.1126/science.1061372

Seymour, D. B., & Calver, C. R. (1995). *Explanatory notes for the time–space diagram and stratotectonic elements map of Tasmania: TASGO NGMA project, sub-project 1: Geological synthesis*. Hobart, TAS: Tasmanian Geological Survey Record 1995/01.

Siégel, C. (2015). *Heat-producing element enrichment in granitic rocks, the role of crustal composition and evolution*. PhD thesis, unpublished. Brisbane, QLD: Queensland University of Technology.

Siégel, C., Bryan, S. E., Allen, C. M., Purdy, D. J., Cross, A. J., Uysal, I. T., & Gust, D. A. (2018). Crustal and thermal structure of the Thomson Orogen: constrains from the geochemistry, zircon U–Pb age, and Hf and O isotopes of subsurface granitic rocks. *Australian Journal of Earth Sciences*, *65*, 967–986. doi:10.1080/08120099.2018.1447998

Sláma, J., Košler, J., Condon, D. J., Crowley, J. L., Gerdes, A., Hanchar, J. M., … Whitehouse, M. J. (2008). Plešovice zircon — A new natural reference material for U–Pb and Hf isotopic microanalysis. *Chemical Geology*, *249*(1–2), 1–35. doi:10.1016/j.chemgeo.2007.11.005

Spandler, M. (1998). *The geology of the Mineral Hill field, central NSW: Igneous evolution and Cu/Au mineralisation*. BSc (Honours) thesis, unpublished. Canberra, ACT: Australian National University.

Valley, J. W. (2005). 4.4 Billion years of crustal maturation: Oxygen isotope ratios of magmatic zircon. *Contributions to Mineralogy and Petrology*, *150*, 561–580. doi:10.1007/s00410-005-0025-8

VandenBerg, A. H. M., Willman, C. E., Maher, S., Simons, B. A., Cayley, R. A., Taylor, D. H., … Radojkovic, A. (Eds.). (2000). *The Tasman Fold Belt in Victoria*. Melbourne, VIC: Geological Survey of Victoria.

Vervoort, J. D., Patchett, P. J., Blichert-Toft, J., & Albarède, F. (1999). Relationships between Lu–Hf and Sm–Nd isotopic systems in the global sedimentary system. *Earth and Planetary Science Letters*, *168*(1–2), 79–99. doi:10.1016/S0012-821X(99)00047-3

Wang, C. Y., Campbell, I. H., Allen, C. M., Williams, I. S., & Eggins, S. M. (2009). Rate of growth of the preserved North American continental crust: Evidence from Hf and O isotopes in Mississippi detrital zircons. *Geochimica et Cosmochimica Acta*, *73*(3), 712–728. doi:10.1016/j.gca.2008.10.037

Watson, E. B., & Cherniak, D. J. (1997). Oxygen diffusion in zircon. *Earth and Planetary Science Letters*, *148*(3), 527–544. doi:10.1016/S0012-821X(97)00057-5

Wellman, P. (1976). Gravity trends and the growth of Australia: A tentative correlation. *Journal of the Geological Society of Australia*, *23*(1), 10–14. doi:10.1080/00167617608728917

Whelan, J., Hergt, J., & Woodhead, J. (2007). Granite–greenstone connection in western Victoria: An example from the Bushy Creek Igneous Complex. *Australian Journal of Earth Sciences*, *54*(7), 975–990. doi:10.1080/08120090701488305

Wiedenbeck, M. A. P. C., Alle, P., Corfu, F., Griffin, W. L., Meier, M., Oberli, F., … Spiegel, W. (1995). Three natural zircon standards for U–Th–Pb, Lu–Hf, trace element and REE analyses. *Geostandards Newsletter*, *19*(1), 1–23. doi:10.1111/j.1751-908X.1995.tb00147.x

Woodhead, J. D., Hergt, J., Shelley, M., Eggins, S., & Kemp, R. (2004). Zircon Hf-isotope analysis with an excimer laser, depth profiling, ablation of complex geometries, and concomitant age estimation. *Chemical Geology*, *209*(1), 121–135. doi:10.1016/j.chemgeo.2004.04.026

Woodhead, J. D., & Hergt, J. M. (2005). A preliminary appraisal of seven natural zircon reference materials for in situ Hf isotope determination. *Geostandards and Geoanalytical Research*, *29*(2), 183–195. doi:10.1111/j.1751-908X.2005.tb00891.x